Depletion of Scleraxis-lineage cells accelerates tendon ECM aging and promotes retention of a specialized remodeling tenocyte population that drives enhanced tendon healing

Antonion Korcari[1,2], Anne E. C. Nichols[1], Mark R. Buckley[1,2], and Alayna E. Loiselle[1,2,*]

[1]Center for Musculoskeletal Research, Department of Orthopaedics & Rehabilitation, University of Rochester Medical Center, Rochester, NY, 14642

[2]Department of Biomedical Engineering, University of Rochester, Rochester, NY, 14627

*Indicates senior author

Keywords: Tendon, extracellular matrix, Scleraxis, aging, tendon healing

Abstract

Tendons connect muscle to bone, enabling skeletal movement and joint stability. During natural aging, tendons exhibit impaired homeostasis, increased risk of injury and impaired healing capacity. Understanding the mechanisms responsible for maintenance of tendon homeostasis and how these mechanisms are diminished with aging is crucial for developing therapeutics that can inhibit age-related impairments in tendon function and healing capacity. Here we show that depletion of *Scleraxis-lineage (Scx^{Lin})* cells, the predominant tenocyte population in adult tendons, recapitulates age-related impairments in cell density, ECM structure and organization. Proteomic analysis demonstrated comparable ECM compositional shifts with Scx^{Lin} depletion in young adult tendon, and wild type (WT) aged tendons and identify the specific ECM components that are lost during disrupted tendon homeostasis. Consistent with this, single cell RNA sequencing demonstrates loss of tenocyte subpopulations associated with "ECM synthesis" in both aging and Scx^{Lin} depletion, identifying the requirement for these cells in maintaining tendon homeostasis. However, aging and Scx^{Lin} depletion results in differential retention of other tenocyte populations, with retention of a specialized remodeling tenocyte population concomitant with mechanically superior healing in Scx^{Lin} depleted tendons relative to WT. In contrast, aged tendon retains a pro-inflammatory tenocyte population, which may drive the impaired healing outcomes observed during aging. Collectively, this study defines Scx^{Lin} cell depletion as a novel model of accelerated tendon ECM aging and identifies tenocyte subpopulations that are associated with disrupted tendon homeostasis and differential healing outcomes.

Introduction

Tendons are dense connective tissues that transmit muscle-generated forces to bone to enable skeletal movement and joint stability. Recent studies from our group and others have demonstrated the presence of multiple tendon resident cell sub-populations with the *Scleraxis-lineage (Scx^{Lin})* cells being the predominant population during adult tendon homeostasis (*1-4*). *Scx*, a basic helix-loop-helix transcription factor, is currently the most well-characterized tendon marker (*5-7*), and is required for normal tendon development (*5, 6*). During adulthood, tendon homeostasis is maintained via ongoing turnover of extracellular matrix (ECM) proteins (*8-14*). Disruptions in tendon homeostasis can lead to the development of tendon pathologies such as tendinopathy, characterized by significant pain, loss of tissue integrity, and permanent decline in tissue performance (*15*). While overuse or repetitive loading in sports or occupational contexts can disrupt homeostasis, natural aging is also associated with significant impairments in ECM structure, organization, and material quality (*16-23*). In fact, tendinopathy prevalence has been shown to significantly increase with age (*24*), making aging a key risk factor for loss of tendon integrity and tendinopathy development. However, the factors responsible for inducing age-related tendinopathy are still not well defined. We have previously shown that short-term depletion of *Scx^{Lin}* cells results in a relatively rapid induction of ECM structural and organizational impairments at multiple hierarchical levels in the flexor digitorum longus (FDL) tendon (*1*), suggesting that *Scx^{Lin}* cells are required to maintain tendon homeostasis during adulthood. However, the long-term impact of *Scx^{Lin}* depletion on tendon homeostasis is unclear, and the specific cellular and ECM components that maintain tendon homeostasis have not been identified. Moreover, while the initial ECM organizational changes that occur with *Scx^{Lin}* cell depletion mimic those that occur during natural aging (*17, 19, 25-27*), it is unknown whether sustained *Scx^{Lin}* cell depletion may induce an accelerated aging phenotype.

In addition to regulating tendon homeostasis, *Scx^{Lin}* cells play an important role in ECM remodeling during healing. Following short-term depletion of *Scx^{Lin}* cells, significant increases in both stiffness and peak load were observed, relative to wildtype (WT) littermates, suggesting a shift towards a more regenerative healing phenotype (*28*). However, the impact of long-term *Scx^{Lin}* cell depletion on the healing process have not been defined. Interestingly, these improvements in healing are in contrast to the effects of aging, which increases the risk of acute tendon injuries and substantially impairs the healing process (*22, 29*). A comprehensive investigation and definition of the basal tendon cell heterogeneity in these different contexts will be crucial to better understand and explain the divergence in healing outcomes.

In the present study our primary objective was to understand the long-term impact of *Scx*^{Lin} cell depletion on tendon health. We then focused on identifying the underlying cell and molecular mechanisms effected by *Scx*^{Lin} cell depletion and how these compositional and mechanistic shifts compared to those observed during natural aging. Finally, we comprehensively defined the shifts in resident tendon cell heterogeneity and the underlying molecular programs driven by *Scx*^{Lin} cell depletion and natural aging. Collectively, this study defines key biological mechanisms that dictate alterations in tendon health and healing capacity.

Materials and Methods

Mice

All animal studies were approved by the University Committee for Animal Resources (UCAR). Scx-Cre mice were generously provided by Dr. Ronen Schweitzer. ROSA26-iDTR$^{F/F}$ (#007900) mice were obtained from the Jackson Laboratory (Bar Harbor, ME, USA). Scx-Cre mice were crossed to ROSA26-iDiphteria Toxin Receptor$^{F/F}$ (DTR$^{F/F}$) mice to generate a model of *Scx*^{Lin} tendon cell depletion (Scx-Cre^{+}; DTR$^{F/+}$; referred to as DTR). Expression of DTR is inhibited prior to Cre-mediated recombination due to the presence of a STOP cassette flanked by loxP sites. After Cre-mediated recombination, the STOP cassette is deleted, resulting in expression of DTR, specifically in *Scx*^{Lin} cells. Thus, administration of diphtheria toxin (DT) in these mice results in apoptosis of *Scx*^{Lin} cells. Scx-Cre^{-}; DTR $^{F/+}$ (WT) littermates were used as controls. DT was administered to both DTR and WT mice. Mouse studies were performed with 6, 9, 12, and 21 month old male and female mice except where otherwise noted, in which case C57BL/6J mice (#664, Jackson Laboratory) were used. All mouse work (injections, surgeries, harvests) were performed in the morning. Mice were kept in a 12 hr light/dark cycle.

Quantification of tendon cell depletion

ScxLin^{DTR} (DTR and WT) mice were anesthetized with Ketamine (100mg/Kg) and Xylazine (4mg/Kg) and then injected with 20 ng of diphtheria toxin (DT; Sigma-Aldrich) for five consecutive days, with DT injections directly into the FDL tendon in the hind paw. Injected hind paws were harvested 3, 6, and 9 months after the final DT injection to assess effects of tendon cell depletion on tendon homeostasis. Hind paws were fixed in 10% Neutral Buffer Formalin (NBF) at room temperature for 72 hr and were subsequently decalcified in Webb Jee EDTA (pH 7.2–7.4) (*30*) for 14 days at room temperature, processed, and embedded in paraffin. Five-micron sagittal sections were utilized for further analysis.

Sections were stained with DAPI to visualize nuclei and imaged using a VS120 Virtual Slide Microscope (Olympus, Waltham, MA). Using ImageJ (*31*), a region of interest (ROI) was drawn at the tendon midsubstance and an area was obtained. For *ScxLin*^{DTR} and WT littermate mice, nuclei within the ROI were manually counted and total nuclei number was normalized to area. An n = 5-7 mice per group were used for quantification.

Second harmonic generation two-photon confocal imaging

Five-micron paraffin sections of DTR, WT, and C57BL/6J hind paws were utilized for second harmonic generation (SHG) imaging. Sections were scanned with a Spectra-Physics MaiTai HP DeepSee Ti:Sapphire Laser, tuned to 1000 nm, under 25x magnification, with a 2.5X optical zoom, with a step size of 0.25 mm. 3D projections of image stacks were generated using the 3D-Project macro in ImageJ and analyzed for collagen fibril uniformity using the inbuilt Directionality macro function. The Directionality macro utilizes Fourier transform analysis to derive spatial orientation of image stacks (*32*). Sections were analyzed from 3 to 5 mice per group.

Quantification of biomechanical properties

FDL tendons at 3, 6, and 9 months post-DT injection were harvested from the hind paws. Specifically, each FDL tendon was carefully separated at the myotendinous junction under a dissecting microscope. The tarsal tunnel was then cut and the FDL tendon was slowly released from the tarsal tunnel, isolated until the bifurcation of the digits and then cut and released. Under the dissecting microscope, any additional connective tissues (e.g., muscle) were removed and the FDL tendon was prepared for uniaxial testing. Two pieces of sandpaper were placed on each end of the tendon and glued together using cyanoacrylate (Superglue, LOCTITE). All the steps above were performed with the tissue periodically submerged in PBS to avoid any potential tissue drying. Each gripped tendon was transferred into a semi-customized uniaxial microtester (eXpert 4000 MicroTester, ADMET, Inc., Norwood MA). The microtester, along with the sample, was transferred to an inverted microscope (Olympus BX51, Olympus) to visualize the tendon and quantify the gauge length, width, and thickness. The gauge length of each sample was set as the end-to-end distance between opposing sandpaper edges and was set the same for all samples tested. The cross-section of the tendon was assumed to be an ellipse, where the width of the tissue represents the major axis and the thickness of the tissue represents the minor axis. Based on the optically measured width and thickness of each tendon, the area of the elliptical cross-section was computed. A uniaxial displacement-controlled stretching of 1% strain per second until failure was applied. Load and grip-grip

displacement data were recorded and converted to stress-strain data, and the failure mode was tracked for each mechanically tested sample. The load-displacement and stress-strain data were plotted and analyzed to determine structural (*stiffness)* and material (*modulus*) properties. Specifically, the slope of the linear region from the load displacement graph was determined to be the stiffness of the tested sample. The slope of the linear region from the stress-strain graph was taken to equal the elastic modulus parameter of each tested tendon. Note that this calculation assumes that stress and strain are uniform within each specimen. A sample size of n=7 animals per group was utilized for biomechanical testing and analysis

Sample Preparation for Mass Spectrometry

Homogenization of each tendon tissue was performed by adding 150 uL of 5% Sodium Dodecyl Sulphate (SDS), 100 mM Triethylammonium bicarbonate (TEAB). Samples were vortexed and then sonicated (QSonica) for 5 cycles, with a 1 minute resting period on ice after each cycle. Lysates were then centrifuged at 15,000 x g for 5 minutes to collect cellular debris, and the supernatant was collected. Next, the total protein concentration was determined by bicinchoninic acid assay (BCA; Thermo Scientific), after which samples were diluted to 1 mg/mL in 5% SDS, 50 mM TEAB. A mass of 25 µg of protein from each sample was reduced with dithiothreitol to 2 mM, followed by incubation at 55°C for 60 minutes. Iodoacetamide was added to 10 mM and incubated for 30 minutes in the dark at room temperature to alkylate the proteins. Phosphoric acid was added to 1.2%, followed by six volumes of 90% methanol, 100 mM TEAB. The resulting solution was added to S-Trap micros (Protifi) and centrifuged at 4,000 x g for 1 minute. S-Traps with the trapped protein were washed twice by centrifuging through 90% methanol, 100 mM TEAB. 1 ug of trypsin was brought up in 20 µL of 100 mM TEAB and added to the S-Trap, followed by 20 µL of TEAB to ensure the sample did not dry out. The cap to the S-Trap was loosely screwed on but not tightened to ensure the solution was not pushed out of the S-Trap during digestion. Samples were placed in a humidity chamber at 37°C overnight. The next morning, the S-Trap was centrifuged at 4,000 x g for 1 minute to collect the digested peptides. Sequential additions of 0.1% Trifluoroacetic acid (TFA) in acetonitrile and 0.1% TFA in 50% acetonitrile were added to the S-trap, centrifuged, and pooled. Samples were frozen and dried down in a Speed Vac (Labconco), then re-suspended in 0.1% trifluoroacetic acid prior to analysis. Three tendons per genotype per timepoint were used for proteomic analysis.

Mass Spectrometry (MS)

Peptides were injected onto a homemade 30 cm C18 column with 1.8 um beads (Sepax), with an Easy nLC-1200 HPLC (Thermo Fisher), connected to a Fusion Lumos Tribrid mass spectrometer (Thermo Fisher). Solvent A was 0.1% formic acid in water, while solvent B was 0.1% formic acid in 80% acetonitrile. Ions were introduced to the MS using a Nanospray Flex source operating at 2 kV. The gradient began at 3% B and held for 2 minutes, increased to 10% B over 6 minutes, increased to 38% B over 95 minutes, then ramped up to 90% B in 5 minutes and was held for 3 minutes, before returning to starting conditions in 2 minutes and re-equilibrating for 7 minutes, for a total run time of 120 minutes. The Fusion Lumos was operated in data-dependent mode, with MS1 scans acquired in the Orbitrap, and MS2 scans acquired in the ion trap. The cycle time was set to 2 seconds. Monoisotopic Precursor Selection (MIPS) was set to Peptide. The full scan was done over a range of 375-1400 m/z, with a resolution of 120,000 at m/z of 200, an AGC target of 4e5, and a maximum injection time of 50 ms. Peptides with a charge state between 2-5 were picked for fragmentation. Precursor ions were fragmented by collision-induced dissociation (CID) using a collision energy of 30% with an isolation width of 1.1 m/z. The Ion Trap Scan Rate was set to Rapid, with a maximum injection time of 35 ms, an AGC target of 1e4. Dynamic exclusion was set to 45 seconds.

MS data filtering

Raw data was searched using the SEQUEST search engine within the Proteome Discoverer software platform, version 2.4 (Thermo Fisher), using the SwissProt mus musculus database. Trypsin was selected as the enzyme allowing up to 2 missed cleavages, with an MS1 mass tolerance of 10 ppm, and an MS2 mass tolerance of 0.6 Da. Carbamidomethyl was set as a fixed modification, while oxidation of methionine was set as a variable modification. The Minora node was used to determine relative protein abundance between samples using the default settings. Percolator was used as the FDR calculator, filtering out peptides which had a q-value greater than 0.01.

Filtered MS data analysis

To identify proteins that were significantly different between two groups, the log2 fold change (FC) and the -log10 of the p-value were plotted in a volcano plot and we utilized the most stringent cut-off parameters of log2FC> 1 and -log10(p-value) >1.3. Significantly decreased proteins among two groups were inserted in PANTHER classification system (*33*) (http://pantherdb.org/) to classify protein type. To understand what types of biological processes (BPs),

molecular functions (MFs), and cellular components (CCs) were shifted on each condition, we inserted all significantly decreased proteins in the gene ontology classification tool DAVID (*34*) (https://david.ncifcrf.gov/). Protein network analysis was performed using the Search Tool for Retrieval of Interacting Genes/Proteins (STRING), v11.0 (*35*), and ECM-related proteins were further classified using MatrisomeDB (*36*) (https://web.mit.edu/hyneslab/matrisome/).

Single cell isolation

A total of 16 FDL tendons per group were pooled together into low glucose Dulmecco's Modified Eagle Medium (DMEM) after harvesting the midsubstance area and digested in Collagenase Type I (Worthington Biochemical, Lakewood, NJ, LS004196) and Collagenase Type IV (Worthington Biochemical, Lakewood, NJ, LS004188) at a final concentration of 5mg/ml and 1 mg/ml, respectively. Young WT tendons were completely digested after two hours, while young DTR and aged C57BL/6J WT tendons after ninety minutes. After digestion, the single-cell suspension was filtered for any potential debris via a 70 μm and a 50 μm cell strainer and resuspended in Dulbecco's Phosphate Buffer Solution (dPBS). Next, the single cell suspension was centrifuged for 10min at 500xg while being at 4 degrees Celsius. After removal of supernatant, the single cell suspension was resuspended in 0.5% Bovine Serum Albumin (BSA).

Single cell RNA sequencing and analysis

Libraries were prepared using a Chromium Single Cell 3 Reagent Kit (version 3, 10X Genomics, Pleasanton, CA) following the directions of the manufacturer. Cells were loaded into the kit and processed using a chromium controller (10X Genomics). Following library preparation and quality control (QC), libraries were sequenced by the UR Genomics Research Center (GRC) using the S2 NovaSeq flow cell system (Illumina, San Diego, CA), generating an average of 65,000 reads per cell for all groups. Raw data 1uality control and downstream analyses were performed with R-4.1.2 and the Seurat package (*37*). Cells with < 200 or > 2,500 genes, as well as cells with > 5% mitochondrial genes were removed from our dataset. After filtering out low quality cells, there were 1,632 cells for the young (6M old) WT group, 1,394 cells for the young (6M old) DTR group, and 1,415 cells for the old (21M old) C57BL/6J WT group. We integrated all three different datasets to determine alterations of different cell subpopulations between groups using the "FindIntegrationAnchors" function (dims = 1:20). The function "IntegrateData" was applied in the anchor set with the default additional arguments. Next, we scaled the data using the "ScaleData" with default parameters and ran principal component analysis (PCA) on the integrated dataset to compute 20 principal components (PCs). Uniform Manifold

Approximation and Projection (UMAP) dimensionality reduction was applied and the Shared Nearest Neighbour (SSN) graph was constructed by utilizing dimensions 1:20 as input feature. To identify cell clusters, we utilized the "FindClusters" function on the integrated dataset at a resolution of 0.5, resulting in 16 different cell clusters. To identify genetic markers of each single cluster and annotate the different clusters to known cell types, we first identified the top differentially expressed genes of each cluster in the heatmap and dot plots ***(Fig. S2)***. Next, we used the "FindAllMarkers" function on upregulated genes only and compared them with a set of literature-defined gene markers via direct literature search as well by utilizing *CellMarker* software (http://bio-bigdata.hrbmu.edu.cn/CellMarker/search.jsp) (*38*). The average gene expression level was calculated across each cluster. The minimum percentage of cells in which the gene is detected in each cluster was set to 50%. The average log2 change threshold was set to at least 0.25. Significance was determined using Wilcoxon rank sum test with p values adjusted based on Bonferroni correction applying all features in the data set ($p\_val\_adj<0.05$). The three tenocytes clusters from the integrated data where subset out from the rest using the "Subset" and "DietSeurat" functions. Next, they were independently re-clustered following the same steps described above, with the following change in computing the principal components. In this section, PCA analysis was ran to compute 30 principal components based on initial QC.

Flexor tendon repair

Complete transection and repair of the FDL tendon was performed as previously described (*39*) in DTR and WT mice at 3M post-depletion (6M old). Mice received an injection of sustained-release buprenorphine (1mg/kg). Mice were anesthetized with Ketamine (60 mg/kg) and Xylazine (4mg/kg). To reduce chances of rupture at the repair site, the FDL tendon was first transected at the myotendinous junction and the skin was closed with a 5–0 suture. This MTJ transection results in a transient decrease in tendon loading, with progressive reintegration of the MTJ observed by D7-10 post-surgery. Next, a small incision was made to the posterior surface of the right hind paw, the FDL tendon was isolated from surrounding tissue and completely transected. The tendon was repaired using 8–0 suture and the skin was closed with a 5–0 suture. Animals resumed prior cage activity, food intake, and water consumption immediately following surgery.

Statistical analysis

Sample sizes were determined based on post-hoc power calculations of previously published work (*3*, *30*). Quantitative data was analyzed via GraphPad Prism and is presented as mean ± standard deviation (SD). Either a student's

t-test or two-way analysis of variance (ANOVA) with Sidak's multiple comparisons test was used as appropriate. Mice were randomly selected for specific experimental outcome metrics prior to the start of an experiment or surgery and quantitative data (ex. DAPI quantification, SHG dispersion levels, biomechanical properties) were analyzed in a blinded manner. For all experiments, an N = 1 represents one mouse. p values ≤ 0.05 were considered significant. * indicates $p<0.05$, ** indicates $p<0.01$, *** indicates $p<0.001$, **** indicates $p<0.0001$.

Results

Scx^{Lin} cell depletion in young adults disrupts tendon homeostasis and mimics the cell density and ECM structural alterations of aging

We have previously shown that local DT injection results in efficient depletion of *Scx*^{Lin} cells in young animals (*1*), however we have not determined whether this cell depletion efficiency is maintained long-term. Therefore, we quantified cell density in DTR mice at 3-, 6-, and 9-months (3, 6, 9M) post-depletion, compared to age-matched DT-treated WT littermates ***(Figure 1A)***. At 3M and 6M post-depletion, there was a respective 57.44% ($p<0.0001$) and 56.21% ($p<0.0001$) reduction in total tendon cell density in DTR tendons relative to the WT control littermates (***Figure 1B, C)***. By 9M post-depletion (12M of age), there was an age-related decrease in the cellular density in WT such that no significant differences in cell density were observed between DTR and WT ($p>0.05$) (***Figure 1B, C)***.

Based on the substantial decline in cellularity that occurred with natural aging in WT tendons, we further tracked changes in tendon cell density from 10-31 months of age in C57BL/6J mice ***(Figure 1D)***. Consistent with the progressive decline in cellularity in WT tendons, cellularity was further decreased at 10M in in C57BL/6J tendons, with a 31.62% ($p<0.0001$) decline in cell density compared to 6M old WT, and a 32.06% decrease ($p<0.0001$) compared to 9M old WT ***(Figure 1D, E)***. At 13 and 31M old, C57BL/6J FDL tendons showed a 43.19% ($p<0.001$) and a 44.42% ($p<0.001$) decrease in total cell density compared to 10M old C57BL/6J FDL tendons, respectively ***(Figure 1D, E)***. Intriguingly, 6M old DTR tendons (3M post-depletion) exhibited a cell density almost identical to 13M and 31M old WT ($p>0.05$) tendons ***(Figure 1D, E)***, suggesting that with *Scx*^{Lin} depletion, young tendons exhibit the same cell density as old and geriatric tendons ***(Figure 1D, E)***.

We then investigated the impact of sustained *Scx*^{Lin} cell loss on long-term tendon homeostasis and collagen ECM organization. Quantification of collagen dispersion via SHG imaging demonstrated significant increase in dispersion (loss

of organization) levels at 3M (39.82%, $p<0.05$), 6M (41.04%, $p<0.01$), and 9M (24.53%, $p<0.05$) post-DT, relative to WT littermates (***Figure 1F, G***), indicative of impairments in tissue structure and organization.

Our next question was how the structure and organization of tendons shifts with natural aging, and whether young (6M old) DTR tendons (3M post-DT) recapitulate potential age-related ECM structural changes. Geriatric 31M old C57BL/6J tendons exhibited significant increases in collagen fibril dispersion compared to 10M (79.3%; $p<0.0001$) and 13M (81.47%, $p<0.0001$) C57BL/6J tendons ***(Figure 1H, I)***, suggesting aging-induced impairments in tendon structure and organization. No differences in dispersion were observed in 3M post-DT (6M old) WT tendons compared to 10M C57BL/6J ($p=0.775$), and 13M C57BL/6J ($p=0.72$) ***(Figure 1H, I)***. In contrast, 3M post-DT (6M old) DTR tendons showed a 45.8% ($p<0.01$) and a 47.63% ($p<0.01$) increase in collagen dispersion compared to 10M and 13M C57BL/6J tendons respectively ***(Figure 1H, I)***, suggesting that young DTR tendons recapitulate age-related deficits in tissue structure and organization. Such recapitulation though was not identical, as geriatric 31M old C57BL/6J tendons still had a significantly higher collagen fibril dispersion (+23.02%, $p<0.05$) compared to 3M post-DT (6M old) DTR tendons ***(Figure 1H, I)***.

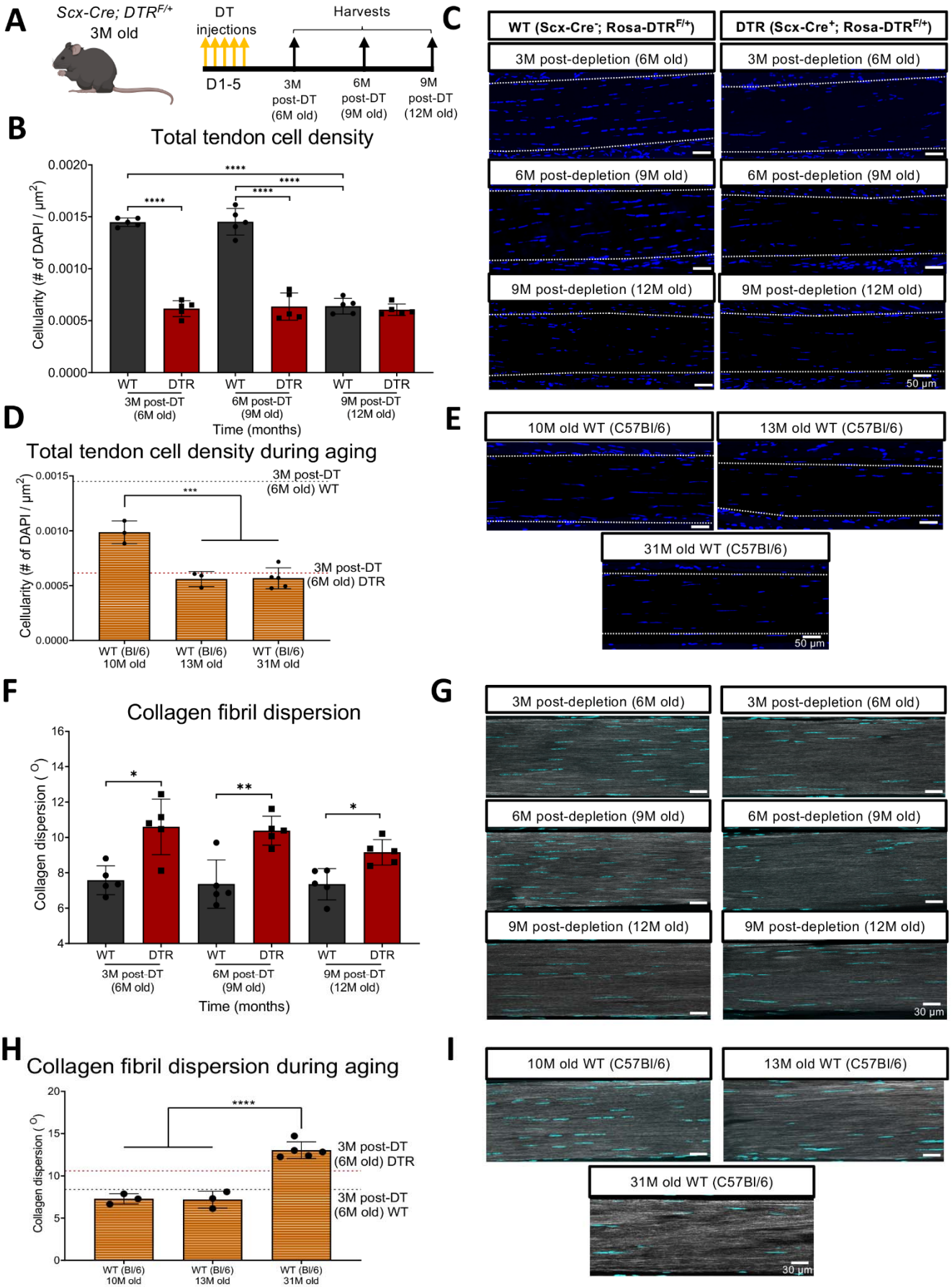

Figure 1. Depletion of *Scx*^{Lin} cell during long-term homeostasis significantly disrupts tendon structure and mechanical properties. (A) 3M old Scx-Cre; DTR$^{F/+}$ mice received five hindpaw injections of DT and were harvested at 3, 6, and 9M post-

depletion. **(B)** Quantification of total tendon cell ($DAPI^+$) density from injected WT and DTR hindpaws at 3, 6, and 9 months post-depletion (6, 9, and 12 months old of age, respectively) within the tendon. **(C)** Representative sections from **(B)**. **(D)** Quantification of total tendon cell ($DAPI^+$) density from C57BL/6J hindpaws at 10, 13, and 31 months old within the tendon. **(E)** Representative sections from **(D)**. **(F)** Quantification of collagen fibril dispersion in WT and DTR samples at 3, 6, and 9 months post-depletion (6, 9, and 12 months old, respectively) and **(G)** representative collagen fibril morphology captured via SHG. **(H)** Quantification of collagen fibril dispersion from C57BL/6J hindpaws at 10, 13, and 31 months old and **(I)** representative collagen fibril morphology via SHG. N=3-5 per genotype. Two-way ANOVA with Sidak's multiple comparisons test used to assess statistical significance of tendon cell ablation and collagen fibril dispersion, * indicates $p<0.05$; ** indicates $p<0.01$; *** indicates $p<0.001$; **** indicates $p<0.0001$.

Scx^{Lin} cells maintain tendon homeostasis by regulating the synthesis of high turnover rate ECM proteins

Given that *Scx*^{Lin} cell depletion induces similar progressive structural ECM changes to those seen in natural aging, we sought to identify the specific biological mechanisms that accompany these structural changes by characterizing the full proteome profile of DTR and WT tendons at 3 and 9M post-depletion (6 and 12M old). At 3M post-depletion, 21 proteins were significantly decreased and 9 proteins were significantly increased, at a minimum abundance level of 2-fold, in the DTR group compared to the WT control littermates (***Figure 2A***), with consistent changes in relative protein abundance levels between biological replicates within each group (***Figure 2B***). To define the broad protein classes that were decreased due to *Scx*^{Lin} cell depletion, we classified all the downregulated proteins using PANTHER (***Figure 2C)***. ECM proteins were the most decreased category, accounting for 26.7% of all downregulated proteins in DTR. (***Figure 2C)***. In addition, cytoskeletal proteins, transporters, and scaffold/adaptor proteins were decreased, though these decreases in inter- and intra-cellular proteins are likely due to a ~60% reduction in cellularity of the DTR samples. Thus, subsequent analysis focused specifically on changes in ECM proteins. To better define the biological mechanisms that are impaired due to depletion of *Scx*^{Lin} cells, we performed functional enrichment analysis of all the downregulated proteins using DAVID (*34*) and found that molecular functions and cellular components exclusive to 'ECM', 'proteinaceous ECM', and 'GAG binding' were significantly impaired in the DTR tendons (***Figure 2D)***. Due to the above ECM-related impairment of tissue homeostasis, we further screened all downregulated proteins and classified which specific ECM-related proteins were decreased in DTR tendons. For the protein screening, we utilized MatrisomeDB and identified a total of 11 ECM proteins that were decreased in DTR tendons (***Figure 2E)***, and they were classified as proteoglycans (36.4%), glycoproteins (36.4%), ECM regulators (18.2%), and ECM-affiliated proteins (9.1%) (***Figure 2F)***. Strikingly, 72.8% of these ECM proteins were high turnover rate glycoproteins and proteoglycans (*8, 10, 11, 40*).

At 9M post-depletion (12M old), 27 proteins were significantly decreased, and 4 proteins were significantly increased in DTR compared to WT littermates (***Figure 2G***), and their relative protein abundance levels were similar among different biological replicates of the same group (***Figure 2H***). Classification of downregulated proteins again

identified ECM proteins as a downregulated class, though ECM proteins accounted for a smaller proportion of down-regulated proteins (11.1%) (***Figure 2I)*** compared to 3M post-depletion (6M old) (26.7%) (***Figure 2C***). Functional enrichment analysis of all downregulated proteins determined that molecular functions and cellular components exclusive to 'ECM', 'ECM structural constituent', and 'proteinaceous ECM' were found to be impaired in DTR (***Figure 2J)***, consistent with those biological processes and cellular components that were impaired at 3M post-depletion in DTR (***Figure 2D)***. Based on the consistent and sustained disruptions in ECM, we classified individual ECM proteins. We found 9 ECM proteins (***Figure 2K)*** that were classified as ECM glycoproteins (50%), ECM-affiliated proteins (30%), collagens (10%), and secreted factors (10%) (***Figure 2L)***. Again, the majority of these ECM-related proteins have a high turnover rate, similar to the findings for the 3M post-depletion timepoint (***Figure 2F)***.

Based on these substantial changes in ECM organization and composition, we also assessed the impact of Scx^{Lin} cell depletion on tendon mechanical integrity (***Fig. S1A)***. No changes in CSA were observed between WT and DTR tendons at any timepoint post-depletion (***Fig. S1B)***. By 3M post-depletion, the stiffness of DTR tendons was not significantly different ($p>0.05$) compared to WT groups (***Fig. S1C)***. By 6M post-depletion, DTR tendons exhibited a trending 23.89% ($p>0.05$) decrease in stiffness compared to WT, and by 9M post-depletion, stiffness was significantly reduced by 29.9% ($p<0.05$) in DTR tendons relative to WT littermates (***Fig. S1C)***. Finally, at 3M post-depletion, DTR tendons had a 19.42% decrease in elastic modulus compared to WT($p<0.01$), with this decrease persisting at 6M post-depletion ($p<0.01$). However, by 9M post-depletion, the elastic modulus between DTR and WT tendons was not significantly different ($p>0.05$) (***Fig. S1D)***. Moreover, the elastic modulus of 12M old WT tendons was decreased by 18.26% ($p<0.05$) and 17.71% ($p<0.05$) compared to that at 6M and 9M old WT tendons (***Fig. S1D)***, suggesting an age-related decrease in tissue material quality.

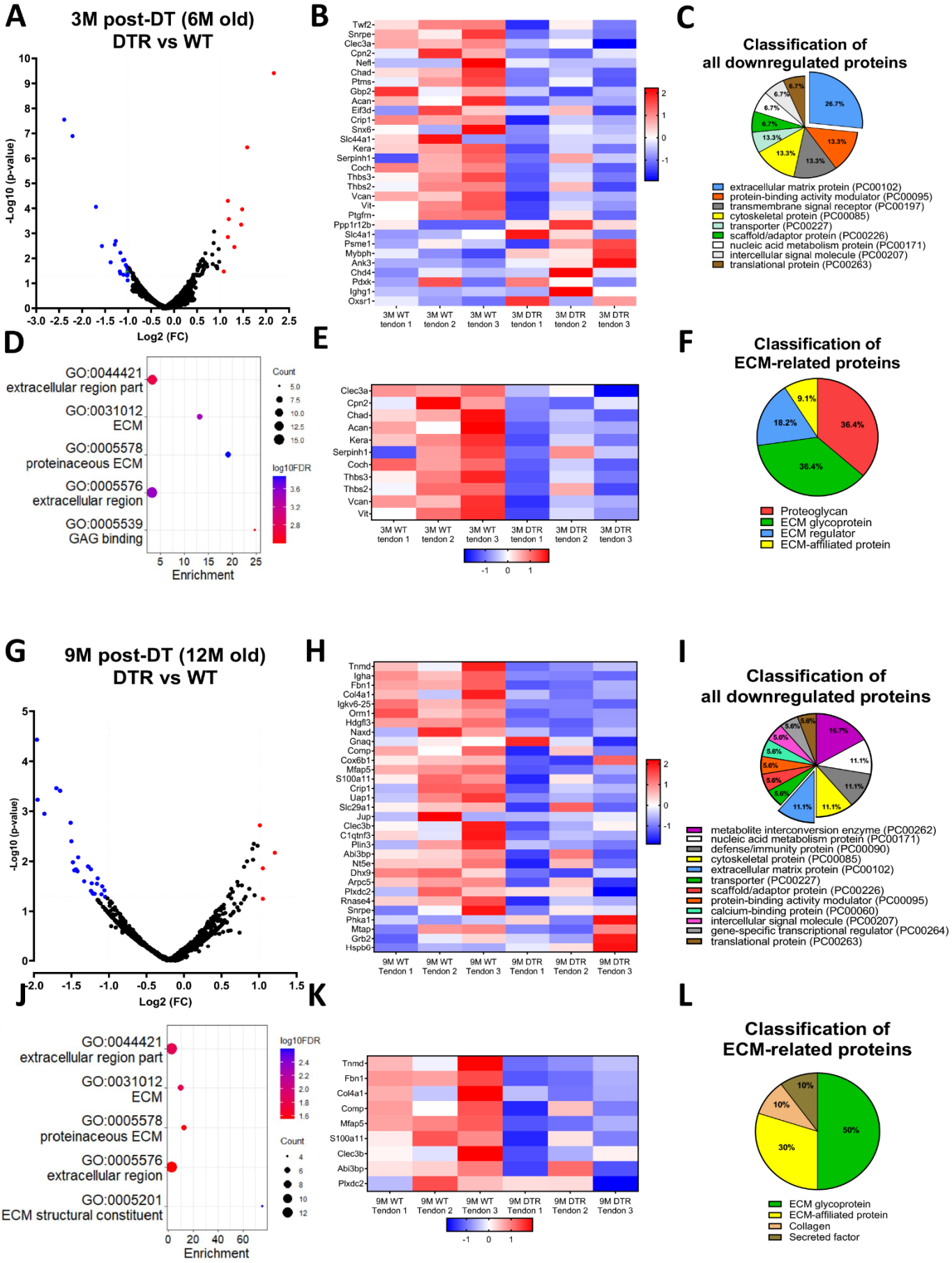

Figure 2. *Scx*^{Lin} cells maintain FDL tendon homeostasis by regulating the synthesis of high turnover rate ECM proteins. (A) Volcano plot visualizing the significantly different protein abundances between DTR and WT groups at 3M post-depletion. **(B)**

Heatmap of differentially abundant proteins in the FDL DTR and WT tendons at 3M post-depletion. **(C)** Classification of all downregulated proteins between the DTR and WT FDL tendons at 3M post-depletion. **(D)** Functional enrichment analysis of cellular components and molecular functions of all downregulated proteins between the DTR and WT FDL tendons at 3M post-depletion. **(E)** Heatmap of all differentially abundant ECM-related proteins between the DTR and WT FDL tendons at 3M post-depletion. **(F)** Classification of all ECM-related downregulated proteins between the DTR and WT FDL tendons at 3M post-depletion. **(G)** Volcano plot visualizing the significantly different protein abundances between DTR and WT FDL tendons at 9M post-depletion. **(H)** Heatmap of differentially abundant proteins in the FDL DTR and WT tendons at 9M post-depletion. **(I)** Classification of all downregulated proteins between the DTR and WT FDL tendons at 9M post-depletion. **(J)** Functional enrichment analysis of all downregulated proteins between the DTR and WT FDL tendons at 9M post-depletion. **(K)** Heatmap of all differentially abundant ECM-related proteins between the DTR and WT FDL tendons at 9M post-depletion. **(L)** Classification of all ECM-related downregulated proteins between the DTR and WT FDL tendons at 9M post-depletion.

Aged tendons exhibit impaired tissue homeostasis similar to young DTR tendons due to a decrease of high turnover rate ECM proteins

Due to the similarities in cell density and structure-function impairments with both DTR and aging, we then asked how the tendon proteome shifts with natural aging (from 6M to 12M of age), and whether aging and *Scx*^{Lin} cell depletion share common biological mechanisms. With natural aging, 16 proteins were significantly decreased, and 9 proteins were significantly increased in 12M old WT compared to 6M old WT ***(Figure 3A)***, and their relative abundance levels were similar among the different biological samples ***(Figure 3B)***. Classification of all downregulated proteins determined that 28.6% were ECM proteins ***(Figure 3C)*** and functional enrichment analysis showed that molecular functions and cellular components related to ‘extracellular region’, ‘ECM’, ‘extracellular space’, and ‘proteinaceous ECM’ were significantly impaired ***(Figure 3D)***.

Based on the consistent and sustained disruptions in ECM with natural aging, a total of 9 decreased ECM proteins were identified ***(Figure 3H)***, and classified as proteoglycans (22.2%), glycoproteins (22.2%), ECM regulators (33.3%), and collagens (22.2%) ***(Figure 3I)***. The majority of the above ECM molecules have a high turnover rate, similar to the findings for the 3M and 9M post-depletion timepoints ***(Figure 2F, L)***. Collectively, these data further support the hypothesis that *Scx*^{Lin} cell depletion in young tendons mimics impairments in ECM-related biological mechanisms that occur during natural aging.

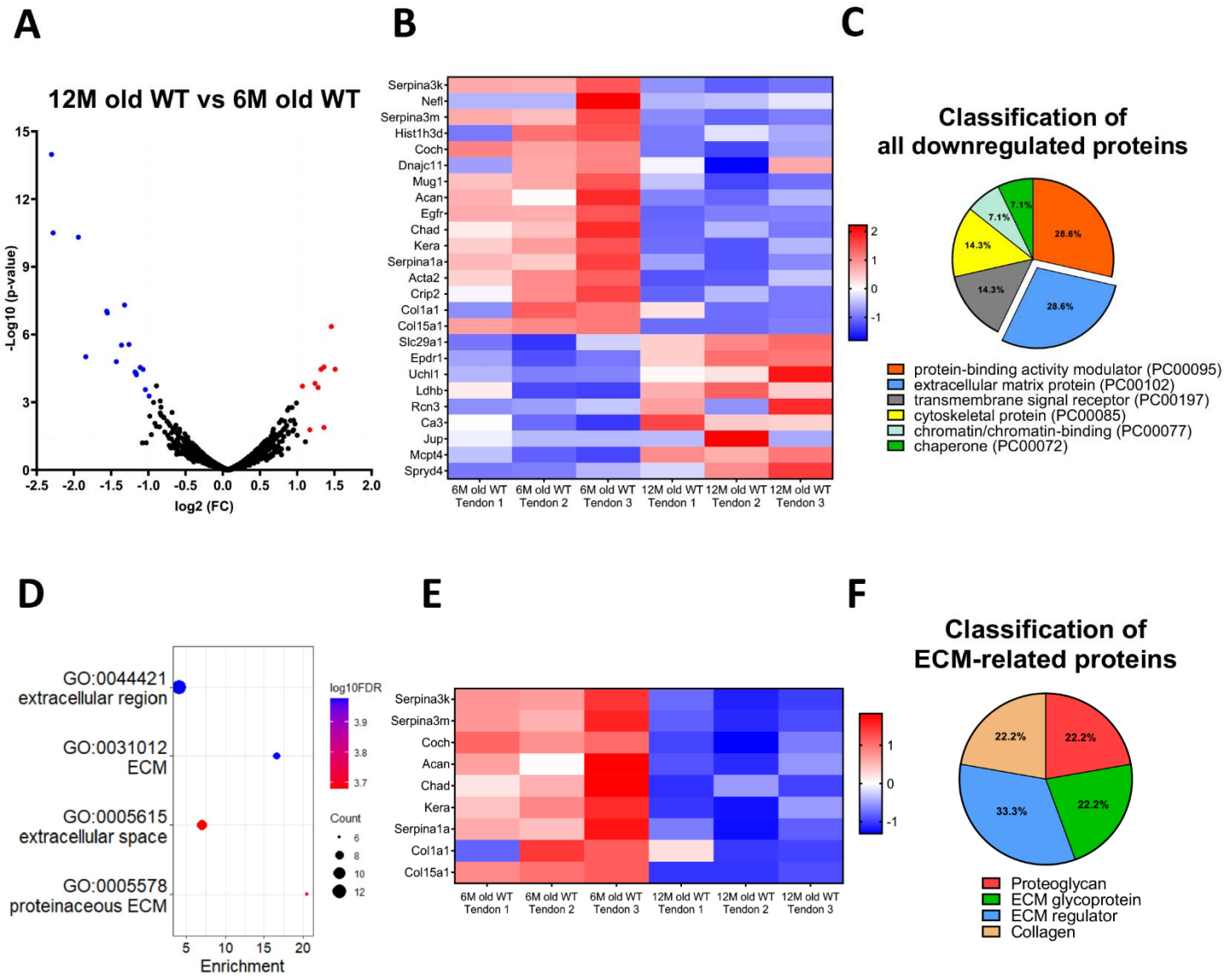

Figure 3. Aged WT tendons exhibit impaired tissue homeostasis similar to young DTR tendons due to a decrease of high turnover rate ECM proteins. (A) Volcano plot visualizing the significantly different protein abundances in WT FDL tendons between 12M and 6M old. **(B)** Heatmap of differentially abundant proteins in WT FDL tendons between 12M and 6M old. **(C)** Classification of all downregulated proteins in WT FDL tendons between 12M and 6M old. **(D)** Functional enrichment analysis of molecular functions and cellular components from all downregulated proteins in WT FDL tendons between 12M and 6M old. **(E)** Heatmap of all differentially abundant ECM-related proteins in WT FDL tendons between 12M and 6M old. **(F)** Classification of all ECM-related downregulated proteins in WT FDL tendons between 12M and 6M old.

Consistent ECM proteome shifts between depletion and aging identify potential ECM regulators of homeostasis

To further validate that DTR and aging induce consistent ECM-related changes, we directly compared the proteome profiles of aged (12M old) WT tendons to young (6M old) DTR (3M post-depletion). Interestingly, the proteomes of aged WT and young DTR tendons were nearly identical with 4 proteins significantly upregulated and 4 significantly downregulated ***(Figure 4A, B)***. No significant differences were identified in any high turnover rate glycoproteins and proteoglycans ***(Figure 4B)*** and functional enrichment analysis of downregulated or upregulated

proteins did not show any significant changes in biological mechanisms between the aged WT and young DTR tendons, suggesting that depletion of *Scx*^{Lin} cells in young tendons recapitulates ECM-related impairments in biological mechanisms happening during natural aging.

To get a better understanding on whether downregulated proteins were associated with each other, we utilized String DB, and found that in DTR tendons, there are two separate groups of downregulated proteins. The first group contains CHAD, CLEC3A, ACAN, KERA, VCAN, THBS2, and THBS3. The other group contains COCH, NEFL, and VIT ***(Figure 4C)***. This suggests that two separate mechanisms of ECM-degradation likely take place upon *Scx*^{Lin} depletion.

With aging, three separate groups of proteins were downregulated**.** The first group contains CHAD, ACAN, COL1A1, COL15A1, ACTA2, KERA and EGFR, the second group contains COCH and NEFL, and the third group contains SERPINA1A, SERPINA3M, SERPINA3K, and MUG1 ***(Figure 4D)***. Interestingly, proteins CHAD, ACAN, and KERA were also in the first group, while COCH and NEFL were in the second protein group in the DTR tendons ***(Figure 4C, D)***, suggesting that very similar mechanisms of ECM degeneration take place both in DTR and aged tendons. Finally, no protein groups were identified in the downregulated proteins between the 12M old WT vs the 6M old DTR tendons ***(Figure 4E)*** further suggesting that with depletion and aging, similar mechanisms of ECM degeneration take place.

Based on these analyses, we identified 4 ECM molecules (COCH, CHAD, KERA, and ACAN*)* that were consistently downregulated with both natural aging and *Scx*^{Lin} cell depletion ***(Figure 4F)***. Classification of the above proteins showed that 75% are proteoglycans and 25% are glycoproteins ***(Figure 4G)***. Moreover, STRING analysis further supported two independent mechanisms of ECM degeneration that occur during both natural aging and with *Scx*^{Lin} depletion, where one process involves decreased expression of CHAD, ACAN, and KERA, while the second is related to decreased COCH expression ***(Figure 4H)***.

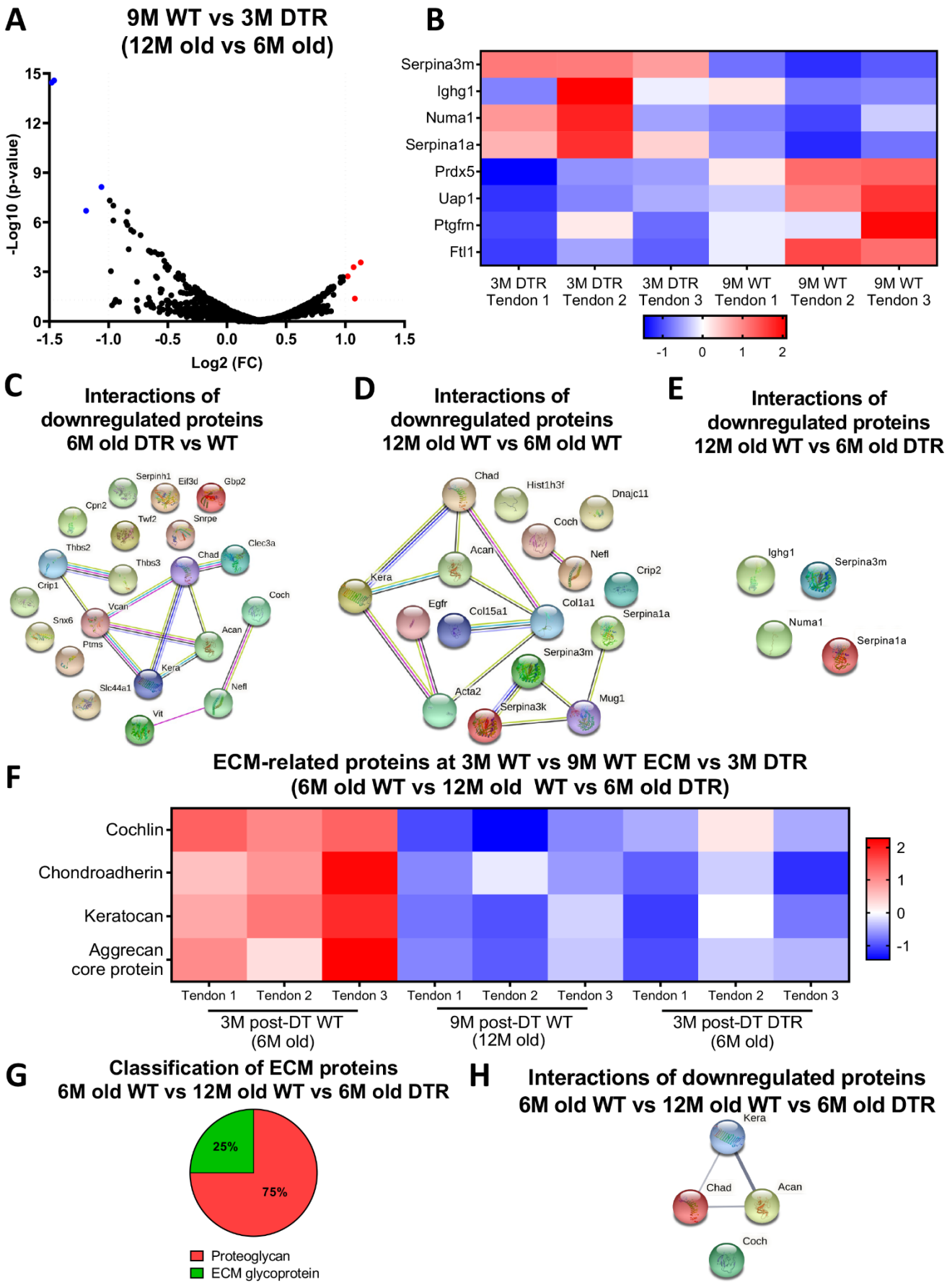

Figure 4. Young DTR FDL tendons exhibit almost identical composition with aged WT FDL tendons and recapitulate similar matrix-related mechanisms of tissue degeneration found during natural aging. (A) Volcano plot visualizing the significantly different protein abundances between 12M old WT and 6M old DTR FDL tendons. **(B)**Heatmap of differentially abundant proteins

between 12M old WT and 6M old DTR FDL tendons. Protein-protein interactions of all downregulated proteins between the DTR and WT FDL tendons at 6M old (**C**), the WT FDL tendons at 12M and 6M old (**D**), and between the 12M old WT and 6M old DTR FDL tendons (**E**). **(F)** Heatmap of ECM proteins in FDL tendons that were differentially abundant between 6M old WT and 12M old WT, 6M old WT and 6M old DTR, and not differentially abundant between 12M old WT and 6M old DTR groups. **(G)** Classification of ECM proteins from (**F**). **(H)** Protein-protein interactions of ECM proteins from (**F**).

scRNAseq demonstrates similar loss and different retention of tenocyte subpopulations with depletion and aging

Given that *Scx*^{Lin} cell depletion in young animals induced similar progressive changes in cell density, ECM structure-function, and composition compared to aged WT tendons, we next asked whether the composition of the tendon cellular landscape was conserved in the context of *Scx*^{Lin} depletion and natural aging, and if there were differences in intrinsic programs between the remaining cell populations in these models. Therefore, we performed scRNA-seq in young 6M old WT and DTR tendons (3M post-DT) and 21M old WT (C57BL/6J) tendons. 21M old WT tendons were used as the 'aged' group as we have previously established that by this age there are age-related impairments in tissue homeostasis and tendon healing response (*29*).

By integrating all the data and using unsupervised clustering and Uniform Manifold Approximation and Projection (UMAP) analysis via *Seurat R* package (*41*), we identified 16 cell types with distinct transcriptomic signatures in the integrated dataset ***(Figure 5A; Fig. S2)***. We annotated three types of tendon fibroblasts (tenocytes) subpopulations (tenocytes 1-3), four epitenon cell populations (epitenon cells 1-4), endothelial, nerve, muscle, pericytes, two red blood cell populations, macrophages, neutrophils, and T-cells ***(Figure 5A; Fig. S2)***. Tenocytes sub-clusters were annotated as such due to the expression of multiple tendon markers (*Scx, Col1a1, Col1a2, Comp, Tnmd, Dcn, Thbs4, Fmod)* ***(Figure 5A; Fig. S2, 3)***. Annotation of epitenon cell clusters is based on additional work from our laboratory that will be published in a separate report ***(Fig. S2)***.

Considering that *Scx*^{Lin} cells are tissue-resident fibroblasts (tenocytes) and that we directly deplete those cells, our primary analysis focused on the impact of depletion and aging on tenocytes specifically. Therefore, we utilized the integrated data from ***Figure 5A***, and re-clustered only the tenocyte subpopulations, resulting in five distinct subpopulations ***(Figure 5B)***, and examined the distribution of these subsets among the different biological samples (6M WT, 6M DTR, 21M WT) (***Figure 5C)***. As expected, the proportion of tenocytes captured was decreased in both 6M DTR and 21M WT groups by 47.22% and 61.5% compared to 6M WT, respectively (***Figure 5D)***.

Next, we found that with both depletion and aging there were significant shifts in the proportion of the five different tenocyte subpopulations. Three populations (tenocytes 1, 2, and 3) were consistently lost with aging and depletion, while different subpopulations were retained in DTR (tenocyte 5) versus aged WT tendons (tenocytes 4) **(*Figure 5E*)**. Tenocytes 1 comprised 37.53% of the total tenocytes in the young WT group, and this population was decreased by 55.99% with depletion (16.51% of total tenocytes being tenocytes 1 in DTR samples), and 88.27% with aging (4.4% of total tenocytes being tenocytes 1 in 21M WT samples). Tenocytes 2 comprised 32.2% of the total tenocytes in the young WT group, and this population decreased by 72.97% with depletion (4.82% of total tenocytes being tenocytes 2 in DTR) and 61.5% with aging (9.12% of total tenocytes being tenocytes 2 in 21M WT). Finally, tenocytes 3 comprised 19.25% of the total tenocytes in the young WT group, and this population decreased by 5.45% with depletion (17.2% of total tenocytes being tenocytes 3 in DTR samples) and 9.39% with aging (15.72% of total tenocytes being tenocytes 3 in 21M WT samples) **(*Figure 5F*)**. In contrast, tenocytes 5 and 4 were disproportionately retained between depleted and aged groups. Tenocytes 5 were the predominant tenocyte subpopulation in the DTR tendons and comprised 59.63% of the total tenocytes in the DTR group. In contrast, it comprised only 2.9% in the young WT and 2.52% in the aged tendons. Tenocytes 4 was the predominant subpopulation in the aged WT tendons, comprising 68.24% of the total tenocytes. In contrast, tenocytes 4 comprised 8.11% and 1.83% of the total tenocytes in young WT and young DTR tendons, respectively **(*Figure 5F*)**.

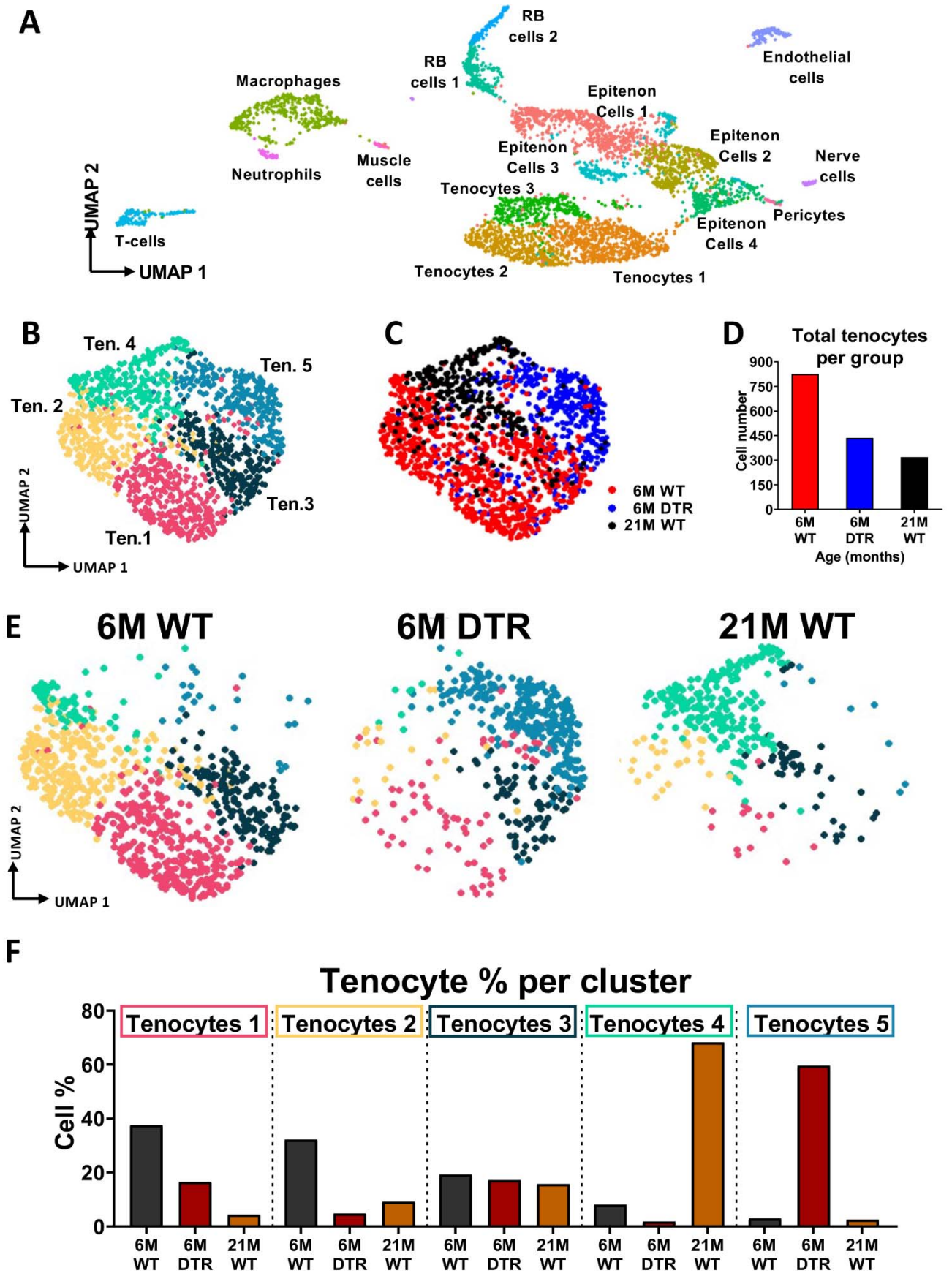

Figure 5. scRNAseq demonstrates both similar and divergent shifts in tenocyte subpopulations composition during depletion and natural aging. (A) UMAP dimensionality reduction revealed 16 distinct cell populations on clustering based on unbiased differential gene expression of the integrated dataset. **(B)** Re-clustering of the tenocyte subpopulations from **(A)** revealed 5 distinct

tenocyte subpopulations based on unbiased differential gene expression of the integrated dataset. **(C)** UMAP plot of tenocytes subpopulations in the integrated data colored based on respective group (black: WT 21M old sample, blue: DTR 6M old sample, red: WT 6M old sample). **(D)** Quantification of the total number of tenocytes found in each group (WT, DTR, 21M WT) **(E)** UMAP plots showing the amount of each tenocyte subpopulation based on the respective group (WT, DTR, 21M old WT (aged)). **(F)** Quantification of cell density for each tenocyte subpopulation normalized by the total number of tenocytes for each respective group

"Specialized structural ECM synthesizers" are lost in DTR and aging, "ECM remodelers" are retained in DTR and "pro-inflammatory and defense responsive" tenocytes are retained in aged WT tendons

To decipher the functions of the different tenocyte subpopulations, we investigated their transcriptomic differences by identifying the top 15 differentially expressed genes for each tenocyte cluster ***(Figure 6A)***, by comparing the average gene expression levels in a given tenocyte cluster to the remaining four clusters, and by performing functional enrichment analyses based on the DEGs for each cluster ***(Figure 6A, B)***. Tenocytes 1 express a significant number of genes that give rise to ECM proteins such as *Col1a1, Col1a2, Fbln1, Fibin, Fmod, Thbs4, Chad, and Coch,* suggesting that this cell cluster is responsible for the synthesis of many tendon ECM proteins ***(Figure 6C, Supplemental Table 1)***. Indeed, when we performed functional enrichment analysis of all the significantly upregulated genes, we found that tenocytes 1 cluster is characterized as a subpopulation responsible for biological processes such as *macromolecule biosynthetic* and *metabolic process, peptide biosynthetic* and *metabolic process, ECM* and *extracellular structure organization, biosynthetic process,* and *anatomical structure development* ***(Figure 6C)***. Based on the DEG and functional enrichment analysis, we further defined tenocytes 1 cluster as a "Specialized structural ECM synthesizer" subpopulation ***(Figure 6C; Fig. S3, S4A-C, Supplemental Table 1)***.

Tenocytes 2 express a significant number of genes related to inflammatory and defense response such as *Csf1, Ccl2, Ccl7, Cxcl14, and Nfkb1,* as well as genes that give rise to ECM proteins such as *Col1a2, Fn1, Thbs2, Coch, and Chad* ***(Figure 6A, Supplemental Table 1)***. Based on functional enrichment analysis, tenocytes 2 cluster is characterized as a subpopulation that is inflammatory (*inflammatory and immune response)*, responsible for defense response and wound healing (*wound healing, response to wounding, and defense response)*, and able to synthesize ECM proteins (*macromolecule biosynthetic* and *metabolic process, peptide biosynthetic process*) ***(Figure 6B)***. Based on the DEG and functional enrichment analysis, we further annotated tenocytes 2 cluster as a "pro-inflammatory and structural ECM synthesizer" subpopulation ***(Figure 6C; Fig. S3, S4A-C, Supplemental Table 1)***.

Tenocytes 3 express genes responsible for synthesis of proteins that remodel the ECM such as *Serpine2, Ecm1, Clec3b, Col3a1,* and *Col5a1* ***(Figure 6A, Supplemental Table 1)***. Based on functional enrichment analysis, tenocytes 3 cluster is characterized as a subpopulation responsible for structural ECM organization and remodeling *(tissue*

remodeling, ECM, and *extracellular fibril organization)*, and for healing response (*wound healing, response to wounding)* ***(Figure 6B)***. Based on the DEG and functional enrichment analysis, we further annotated tenocytes 3 cluster as an "ECM organizer and remodeler" subpopulation ***(Figure 6C; Fig. S3, S4A, D, E, Supplemental Table 1)***.

Tenocytes 5 express genes responsible for ECM organization and remodeling in both homeostasis and injury, such as *Mmp2, Col3a1, Edil3, Col4a2,* and *Mfap5* ***(Figure 6A, Supplemental Table 1)***. These findings were further validated when we performed functional enrichment analysis in all DEGs upregulated in tenocytes 5 compared to the rest tenocytes subpopulations. In specific, tenocytes 5 cluster was shown to be responsible for biological processes related to *response to wounding, ECM organization, extracellular structure organization, extracellular fibril organization* and *tissue remodeling* ***(Figure 6B)***. Based on the above data, we further annotated tenocytes 5 cluster as an "ECM organizer and remodeler". ***(Figure 6C; Fig. S3, S4A, D, E, Supplemental Table 1)***.

Finally, tenocytes 4 express a significant number of genes related to inflammatory and immune responses such as *IL6, Cxcl1, Icam1, Ccl2, Ccl7, and Cxcl12*. Functional enrichment analysis of upregulated DEGs found that tenocytes 4 are responsible a plethora of inflammatory and immune-related processes (*regulation of IL12 production, IL6 production, innate immune response, defense response, and inflammatory response)* ***(Figure 6B).*** Based on all the above data, we further annotated tenocytes 4 as a "pro-inflammatory and defense responsive" subcluster ***(Figure 6C; Fig. S3, S4A-C, Supplemental Table 1)***.

We found that in both 6M DTR and 21M WT aged tendons, there was a decrease in the "specialized structural ECM synthesizer" (tenocytes 1), the "pro-inflammatory and structural ECM synthesizer" (tenocytes 2), and the "ECM organizer and remodeler" (tenocytes 3) populations, corroborating our proteomics data of similar compositional shifts, since there is a similar loss of cells that typically would maintain the synthesis of high turnover rate ECM proteins. Moreover, only the "ECM organizer and remodeler" (tenocytes 5) were retained in the 6M DTR tendons and the "pro-inflammatory and defense responsive" (tenocytes 4) were retained in the 21M WT aged tendons ***(Figure 6D, E)***, suggesting that DTR tendons may respond better to injury due to the presence of a specialized remodeling tenocyte population, in contrast to aged WT tendons that exhibit impaired healing, perhaps due to an exuberant inflammatory response and minimal reorganization/remodeling capacity. Interestingly, scRNAseq analysis of only the young (6M old) WT resulted in three tenocyte subclusters **(*Fig. S3),*** while in the integrated data, there were five tenocyte subpopulations. Based on DEG analysis and proximity in UMAP graphs, it is possible that there are programmatic shifts of tenocytes 2 to tenocytes 4 **(*Fig. S5)*** and tenocytes 3 to tenocytes 5 **(*Fig. S6)***.

Finally, considering the four newly identified ECM molecules (COCH, CHAD, KERA, and ACAN core) that were consistently decreased in both DTR, and aged tendons based on unbiased proteomic analysis ***(Figure 4F)***, we asked which specific tenocyte subclusters were actively expressing the genes responsible for the production of these proteins. ScRNA-seq analysis demonstrated that all five tenocyte clusters actively expressing *Coch* and *Chad* ***(Fig. S7)***. In tenocytes 1, 2, and 3, expression of both *Coch* and *Chad* was decreased in DTR and 21M aged WT tendons compared to young WT. Tenocytes 5 and 4 showed higher expression of *Coch* and *Chad* in young DTR and 21M WT tendons, respectively. In terms of *Acan*, in tenocytes 1 and 2, only young WT tendons were expressing *Acan* (less than 2 % of the cluster). In tenocytes 5, only the young DTR tendons expressed Acan (less than 4% of the cluster. No expression was found at tenocytes 4 and less than 2% expression in tenocytes 3 ***(Fig. S7A-H)***. In terms of *Kera* expression, tenocytes 1 and 2 showed a decrease in DTR and aged WT compared to young WT. In tenocytes 5, *Kera* expression was retained in DTR tendons (~6% of the cluster), while in tenocytes 4, it was retained in 21M old WT. Finally, there was almost no *Kera* expression in tenocytes 3 ***(Fig. S7A-H).*** Together, these data suggest that loss of COCH, CHAD, KERA, and ACAN in DTR and aged WT tendons is primarily due to the death of cells that express the above molecules in the transcript level.

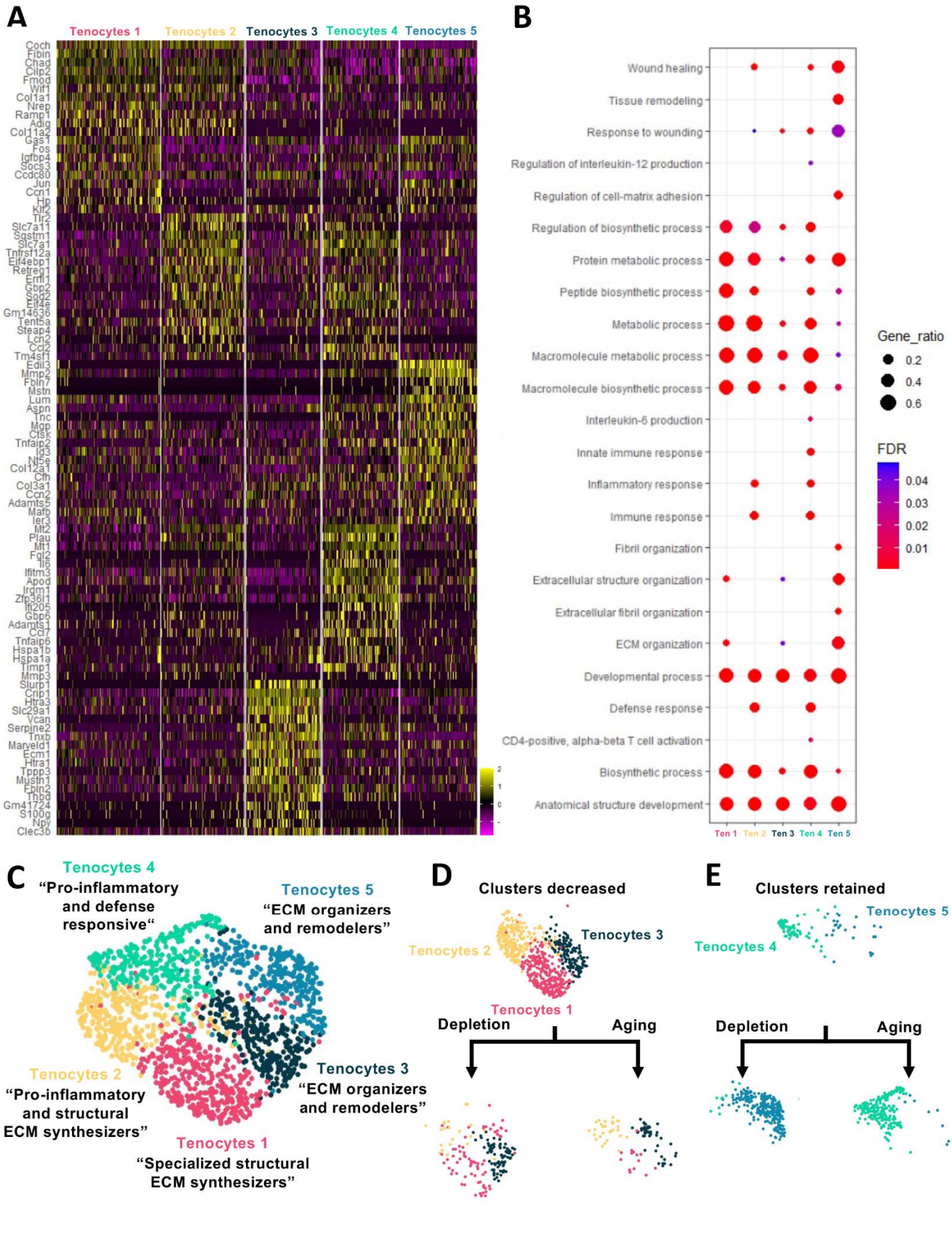

Figure 6. A loss of structural ECM synthesizers is identified in both young DTR and aged WT tendons, while ECM organizers/remodelers and pro-inflammatory/defense responsive tenocyte subclusters are disproportionately retained in DTR and aged WT tendons. (A) Top 20 differentially expressed genes between tenocytes 1 to 5 subclusters visualized by heatmap. **(B)** Functional enrichment analysis of biological processes upregulated in each tenocyte subpopulation.**) (C)** UMAP of all 5 tenocyte subpopulations annotated based on their top DEGs and the biological processes they follow. **(D)** UMAP of all three tenocyte clusters (tenocytes 1, 2, and 3) that were found to decrease both in DTR and aged tendons. **(E)** UMAP of the two tenocyte clusters (tenocytes 5 and 4) that were found to be disproportionately retained in aged and DTR tendons, respectively.

Young DTR tendons heal with improved biomechanics compared to young WT tendons

Based on the increased retention of "ECM organizers and remodelers" in young DTR and the significant number of "pro-inflammatory, immune responsive" in young WT tendons, we hypothesized that 6M DTR tendons would heal with improved structural and material properties compared to 6M WT tendons. To test this hypothesis, we performed total transection and repair surgery in WT and DTR tendons (3M post-depletion) and harvested them at D14 post-surgery for biomechanical testing ***(Figure 7A)***. As hypothesized, DTR tendons healed with improved structural and material biomechanical properties compared to WT tendons ***(Figure 7C-E)***. Specifically, while there were no significant differences in CSA between the DTR and WT tendons ***(Figure 7C)***, both stiffness and elastic modulus in DTR tendons were significantly higher compared to WT littermates ***(Figure7D, E)***. In terms of stiffness, DTR tendons demonstrated a 114.6% ($p<0.01$) increase compared to WT tendons ***(Figure 7D).*** Finally, DTR tendons demonstrated a 108.45% ($p<0.05$) improvement in elastic modulus compared to WT tendons ***(Figure 7E)***. Collectively, these data suggest that in DTR tendons, the "ECM organizers and remodelers" tenocyte subpopulations (clusters 3 and 5; 77% of the total tenocytes) played a significant role in organization and remodeling of the injured tendon area, translating in improved structural and material properties, compared to WT tendons where the lack of the above cells (less than 20% of the total tenocytes) in combination with the presence of pro-inflammatory tenocytes result in the formation of an unorganized and mechanically weak scar tissue with a prolonged inflammatory response, and thus in impaired healing quality.

Consistent with these data, we have previously shown that DTR tendons demonstrated improved healing compared to WT littermate controls (*30*); however, in that study, the injury was induced 10 days after depletion. Therefore, it was important to determine whether longer-term depletion of Scx^{Lin} resulted in the same functional improvements, which was the case here ***(Figure 7C-E)***. Given these consistent improvements in healing following Scx^{Lin} depletion, we utilized bulk RNAseq data analysis from this previous study (*30*) to determine if there was an enrichment in genes associated with the tenocytes 5 "ECM organizers and remodelers" cluster, since this is the predominant cluster that is retained in DTR tendons. Indeed, we identified ten genes (*Fbln7, Aspn, Mfap2, Col3a1, Thbs4, Ogn, Mfap5, Lama4,*

Thbs1, and Lum) associated with tissue remodeling and specific to tenocytes 5, that were highly and significantly expressed in D28 DTR tendons relative to WT repairs (*30*) ***(Figure 7F-H)***.

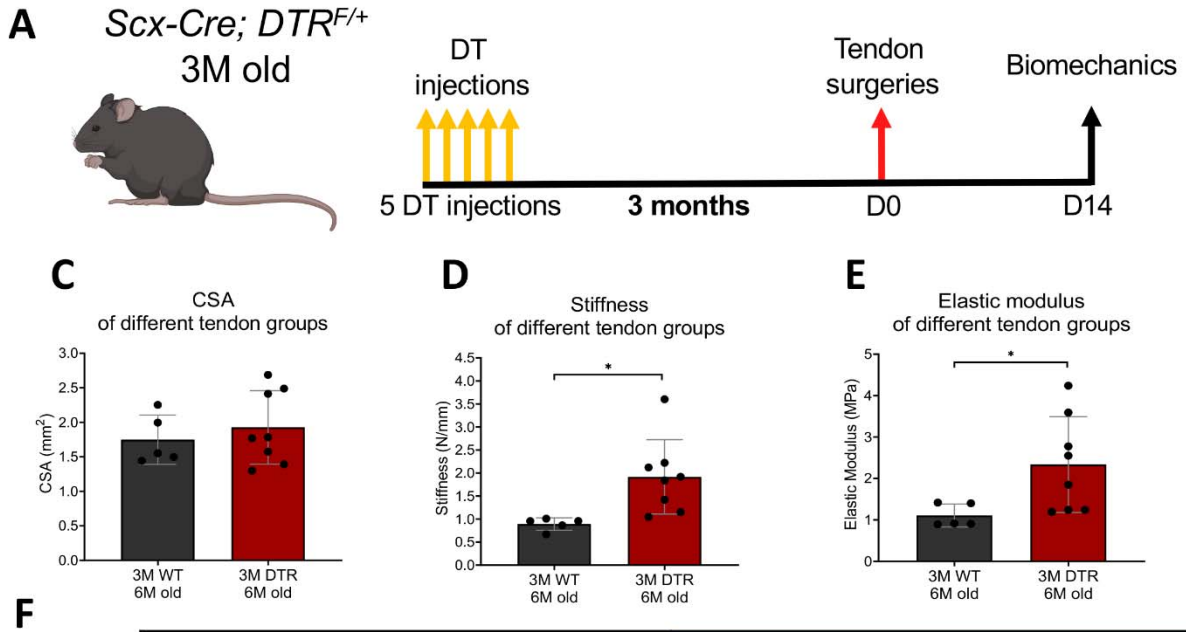

F

	Enrichment of genes associated with tissue remodelling in tenocytes 5 "specialized remodelers" (scRNAseq data in this study)		Enrichment of genes associated with tissue remodelling in D28 DTR tendons with improved healing (Bulk-seq dataset, Best and Korcari, eLife, 2021)	
Gene name	**avg_log2FC**	**p_val_adj**	**avg_log2FC**	**p_val_adj**
Fbln7	1.00	4.8660E-74	0.78	0.002330
Aspn	1.68	8.6299E-46	0.84	0.007556
Mfap2	0.55	8.4151E-19	0.47	0.013072
Col3a1	0.91	1.9191E-14	0.65	0.005567
Thbs4	0.59	6.3953E-09	0.84	0.000057
Ogn	0.66	1.0294E-03	0.64	0.004079
Mfap5	0.73	2.9735E-03	0.75	0.000053
Lama4	0.27	1.4667E-03	0.34	*0.081572*
Thbs1	0.84	2.5154E-04	0.49	*0.099587*
Lum	1.74	3.8544E-51	0.35	*0.130133*

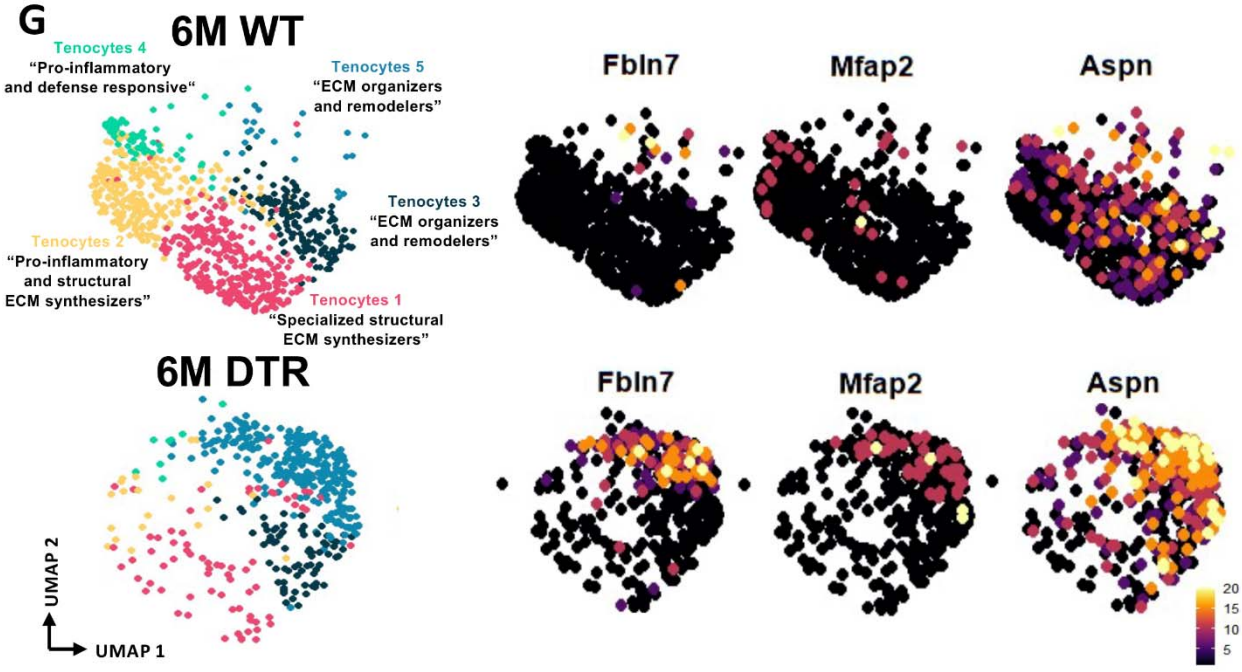

Figure 7. Young DTR tendons heal with improved structural and material properties than young WT tendons. (A) Young adult mice at 3M old received hindpaw injections of DT for 5 consecutive days, underwent FDL tendon surgery repair 3 months after the

final DT injection, and were harvested at 14 days post-surgery. (**B**) Upper middle-aged C57BL/6J mice at 15M old underwent FDL tendon surgery repair and were harvested at 14 days post-surgery. CSA (**C**), stiffness (**D**), and elastic modulus (**E**) of 3M post-depletion (6M old) WT, DTRFDL tendons at 14 days post-surgery. **(F)** Genes associated with tissue remodeling that were found to be significantly expressed both in tenocytes 3 subpopulation on young DTR tendons in this study as well as in D28 post-surgery DTR tendons that were healed regeneratively from *Best* and *Korcari, eLife* 2021. N=5-11 per genotype. One-way ANOVA followed by Tukey's post-hoc analysis was used to compare CSA, stiffness, and elastic modulus between the 3M post-depletion (6M old) WT, DTR, and 15M old WT C57BL/6J FDL tendon groups. **(G)** UMAP graph of the annotated five tenocyte subclusters in the 6M WT and DTR tendons and UMAP graph of the expression levels of *Fbln7, Mfap2, and Aspn* that were significantly upregulated in tenocyte 5 subcluster as well as in D28 post-surgery DTR tendons that were healed regeneratively from (*30*).

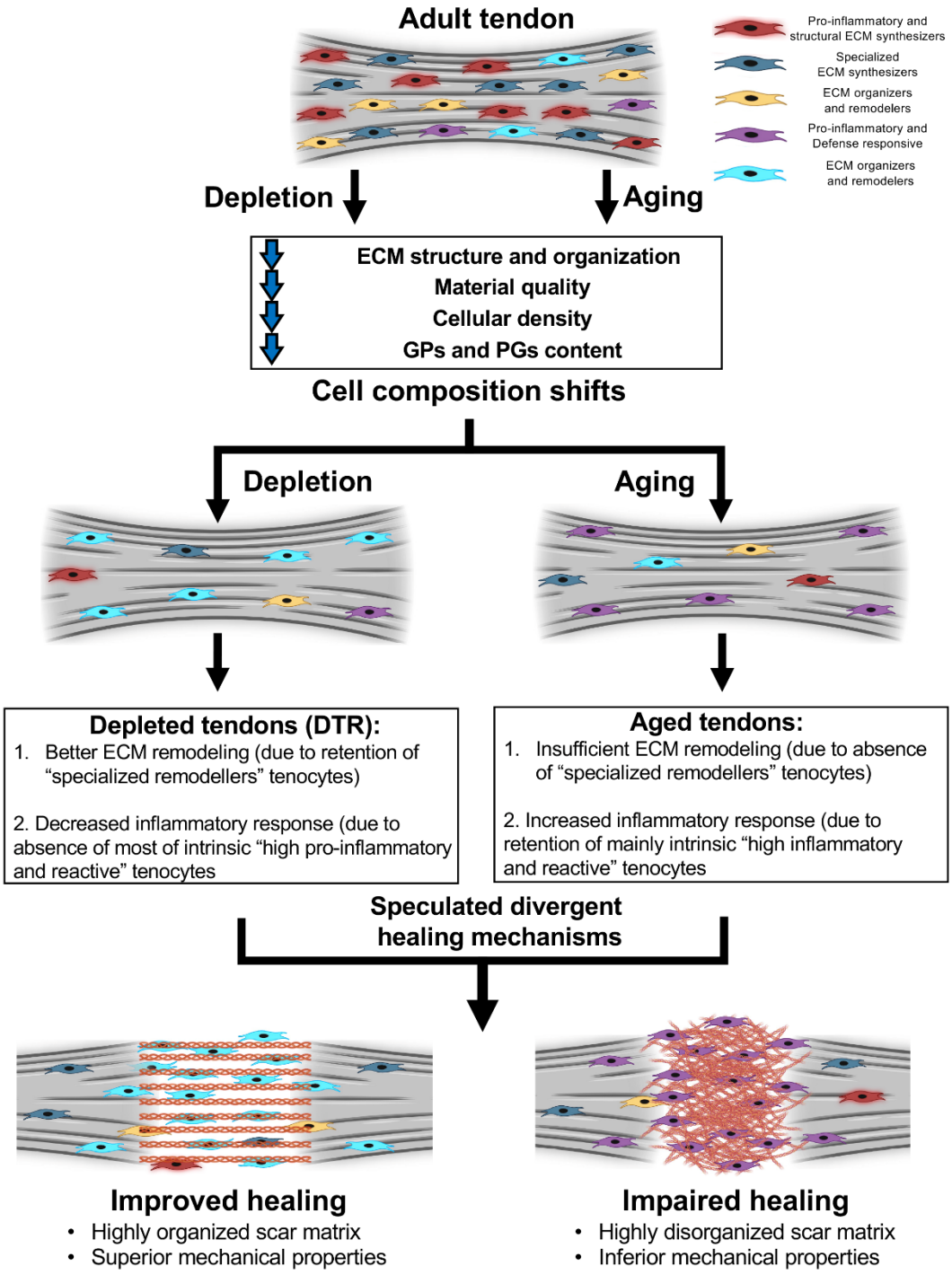

Figure 8. Schematic highlighting key findings and proposed models for divergent healing responses in young depleted vs aged tendons. Both young DTR and aged WT tendons have similar decreases in tissue structure, organization, material quality, and total

cell density. They also follow the same mechanism of ECM degeneration via a substantial decrease in the number of proteoglycans and glycoproteins with high turnover rate. However, in terms of cell composition shifts with depletion and natural aging, young DTR tendons are comprised mainly of tenocyte subpopulations that are specialized in tissue remodeling. What is more, young DTR have little to no inflammatory/reactive tenocytes. In contrast, old WT tendons are comprised predominantly of inflammatory tenocyte subpopulations and have little to no tissue remodeling tenocytes. We speculate that these significantly different cellular compositions are some of the main causes resulting in divergent healing responses, with young DTR tendons showing improved healing while old WT tendons exhibiting impaired healing response.

Discussion

In this study, we showed that long-term depletion of *Scx*^{Lin} cells disrupts tendon homeostasis and recapitulates many age-related disruptions of tendon homeostasis including decreased cell density, deficits in ECM organization, alterations in ECM composition, and mechanical impairments. Proteomic analysis demonstrated that the ECM composition between young DTR and aged WT tendons was very similar suggesting that depletion of *Scx*^{Lin} cells mimics ECM-related mechanisms of tissue impairment happening during natural aging. Moreover, scRNA-seq analysis demonstrated a conserved loss of "structural ECM synthesizers" tenocytes subclusters in both DTR and aging, consistent with impairments in synthesis of high turnover rate ECM proteins and loss of tendon homeostasis. Intriguingly, we found that young DTR tendons almost exclusively retained the "ECM organizer and remodeler" tenocyte population, while both young WT and aged C57BL/6J tendons maintained a substantial population of "pro-inflammatory and defense responsive" tenocytes. Collectively, these data identify a population-based mechanism of the divergent healing outcomes that are observed between young WT and DTR tendons, and between young and aged C57BL/6J tendons (*29*). More specifically, these data suggest that enhanced tissue remodeling may underly the improved healing observed with *Scx*^{Lin} cell depletion, while age-related impairments in healing are due to a combination of the loss of the "ECM organizer/remodeler" population and retention of the "pro-inflammatory" tenocyte population.

While we have previously shown that this *Scx*^{Lin} depletion strategy results in an initial ~60% decrease in tendon cell density (*30*), it was unknown whether this was a sustained or transient depletion event that eventually results in re-population of the tendon via compensation by non-depleted populations. Indeed, this model results in sustained cell depletion, thus allowing assessment of the long-term impact of *Scx*^{Lin} cell deficiency. It is important to note that this model likely depletes any "progenitor" cell populations due to the use of non-inducible Scx-Cre, further inhibiting any potential cellular rebounding post-depletion. Moreover, we observed that *Scx*^{Lin} cell depletion resulted in almost identical cellular density with older (12M old) and geriatric (31M old) tendons, indicating that with depletion, there is an acceleration of the natural age-related tendon cell death. These findings are consistent with previous studies that demonstrate consistent age-related declines in tendon cell density that are conserved across anatomically distinct tendons and different animal models

(*42-44*). In addition to mimicking age-related declines in cell density, *Scx*^{Lin} cell depletion also recapitulated age-related impairments in tendon ECM structure, organization, and composition. While age-related declines in tendon ECM structure and organization have been found across tendons (e.g., Achilles, flexor, patellar, and supraspinatus) and animal models (e.g., mouse and rabbit) (*17, 19, 25, 42, 45*), the compositional shifts that underpin these structural changes are less well-defined. Our findings demonstrate that *Scx*^{Lin} cells are required to directly regulate the synthesis and maintenance of multiple high turnover rate glycoproteins (GPs) and proteoglycans (PGs), which are crucial to maintain tendon structure-function, since their decrease results in significantly impaired collagen fibril organization and biomechanical properties. In agreement with our findings, previous studies have shown, via genetic knock out models, that high turnover rate GPs and PGs are required to maintain tissue homeostasis during adulthood in tissues such as tendons as well as bone, cartilage, and skin (*46-59*). However, these studies have been descriptive in terms of understanding the role of a specific ECM molecule in tissue homeostasis. In contrast, for the first time, we show that the "master-regulator" of multiple ECM-related proteins during tendon homeostasis are the *Scx*^{Lin} cells. Another important finding is the recapitulation of age-related compositional changes in young DTR tendons. Similar to this, other studies have found that aged tendons demonstrated a decrease in abundance levels of ECM-related proteins (*18, 19, 21, 22, 40, 42, 45, 60-63*); however, in this study, we provide the specific underlying molecular mechanisms that are lost with tendon aging. More specifically, based on our proteomic analysis, we identified four novel ECM molecules (COCH, CHAD, KERA, and ACAN) that exhibited conserved downregulation following Scx^{Lin} cell depletion and aging, suggesting that they may be key regulators of tissue homeostasis during adulthood.

Based on our scRNAseq results, we identified five distinct tenocytes subpopulations, and by combining the DEGs and GO analyses, we annotated them as "specialized structural ECM synthesizers", "pro-inflammatory and structural ECM synthesizers", "ECM organizers and remodelers 1", "Pro-inflammatory and defense responsive", and "ECM organizers and remodelers 2". Interestingly, our data suggest a potential programmatic shift of tenocytes 3 and 5 with depletion as well as tenocytes 2 and 4 with natural aging. In specific, relative DEG analysis between tenocytes 3 and 5 showed that tenocytes 3 (retained in WT) are more specialized to the remodeling and biosynthesis of different PGs and GPs. In contrast, tenocytes 5 (retained in DTR) have become much more specialized in the remodeling and organization of the ECM and are not as biosynthetic as tenocytes 3. Based on these data, it seems that with depletion, the "ECM organizers and remodelers 1" tenocytes 3 shift their roles from synthesizing multiple GPs and PGs to becoming more active in the organization and remodeling of the current matrix they are in. Another potential programmatic shift seems to

take place between tenocytes 2 and 4. Tenocytes 2 (retained in young WT) seem to be responsible for the biosynthesis of ECM proteins, while tenocytes 4 (retained in old WT) are more inflammatory and less biosynthetic compared to tenocytes 2. It seems that with natural aging, the "pro-inflammatory and structural ECM synthesizers" tenocytes 2, become more inflammatory and less biosynthetic. In agreement with our findings, recent studies have also demonstrated tissue-resident fibroblast heterogeneity in tendons (*2, 4, 64, 65*). Kendal *et al*., performed scRNAseq analysis in human tendons and found two tenocyte subclusters that express pro-inflammatory markers such *Cxcl1, 6,* and *8* and *Ccl2* (*4*). Lehner *et al*., also demonstrated the existence of resident tenocytes expressing pro-inflammatory markers *Cx3Cl1/Cx3cr1* in healthy tendons from both mouse and human (*66*). These studies further support our findings of tenocytes 2 and 4 being characterized by pro-inflammatory genetic signatures. Moreover, scRNAseq analysis of fibroblast heterogeneity in healthy human skin demonstrated that two of the four fibroblast subclusters had specific functional roles related to collagen and ECM organization, highlighting their potential roles for tissue organization and remodeling after injury (*67*).

The loss of "structural ECM synthesizers" tenocytes in both young depleted and aged WT tendons support the similarities we noticed earlier in impairments of structure-function and ECM-related biological mechanisms with both depletion and natural aging. In specific, these data further supports that the "structural ECM synthesizers" are the key player cell populations required for producing multiple ECM proteins that are crucial for maintenance of tendon homeostasis, Surprisingly, young DTR tendons were predominantly comprised of "ECM organizers and remodelers" suggesting their potential superior remodeling ability during tendon injury. Consistent with this, both short (10 days)(*1*) and long-term (3M) depletion of Scx^{Lin} cells prior to injury results in improved biomechanical properties relative to WT littermates, and demonstrated significantly elevated expression of genes associated with the "ECM organizers and remodelers" tenocyte population, and suggesting these cells as a critical driver of enhanced tendon healing.

Here, we identified that aged WT tendons were comprised of almost no "ECM organizers and remodelers" and a significant number of "pro-inflammatory" tenocytes, suggesting that these alterations in composition of the tenocyte environment may be a crucial factor driving the insufficient healing response in aged tendon. We have previously challenged aged FDL tendons with a full transection and repair surgery and found that 22M old C57BL/6J tendons do indeed heal with impaired biomechanical properties compared to young (4.5M) old C57BL/6J counterparts (*29*). In support of our scRNAseq findings, others have previously shown the existence of a chronic and progressive tissue intrinsic pro-inflammatory phenotype, also termed "inflammaging" (*68*), as well as a conserved decrease in ECM components across multiple tissues and animal models (*67, 69-71*). More specifically, in aged skin, multiple dermal

fibroblast subpopulations exhibit a significant decrease in ECM gene expression in conjunction with an increase in expression of inflammatory and immune-related genes, collectively suggesting shifts in the tissue-resident fibroblast environment as a key feature of tissue aging (*67, 71*). Our findings here demonstrate, for the first time, that a combination of decreased expression of ECM genes and an increased pro-inflammatory environment, also happens in tendons, and play a major role in the loss of structure-function and composition.

Finally, we showed that DTR tendons heal with superior structural and material properties compared to their WT littermates. Given that our scRNAseq results indicate DTR tendons to be comprised almost exclusively of "ECM organizer and remodeler" tenocytes 3, we believe that this newly identified cell population is responsible for the better organization of the newly formed ECM in the healing tendon, which then translates in a stronger healed tissue. Indeed, we identified multiple tenocytes 5 specific-ECM genes (*Fbn7, Aspn, Mfap2, Col3a1, Thbs4, Ogn, Mfap5, Lama4, Thbs1, and Lum)* to be highly expressed in the bulk RNA-seq dataset of D28 post-surgery DTR tendons, previously shown to demonstrate a regenerative healing phenotype relative to WT littermates (*30*).

One limitation of the study is that the *Scx-Cre; DTR* $^{F/+}$ targets all *Scx*^{Lin} cells, and the *Scx*^{Lin} is known to contribute to tissues in addition to tendon (*e.g.* bones and muscle) (*72, 73*). However, our initial plans to deplete *Scx*^{Lin} cells by utilizing the inducible *Scx-Cre*^{ERT2} crossed to the diphtheria toxin A-subunit gene (DTA) mouse model, resulted in insufficient cell depletion. A second limitation is that we have only assessed healing in WT and DTR at D14, however, we have previously shown that *Scx*^{Lin} depletion immediately (10 days) prior to injury improves healing at D28 (*30*). Finally, although we suggest that young DTR and aged WT tendons would exhibit divergent healing outcomes because of the different tenocyte sub-populations retained in each group, we have not examined these populations in healing tendon, and it is not yet clear how the overall cell environment shifts in these different contexts during the healing process, which will be the focus of future studies.

In this study, we demonstrated that during adulthood, multiple subpopulations of *Scx*^{Lin} cells are required for the direct synthesis and maintenance of homeostatic levels in multiple known and newly identified ECM-related proteins, crucial for tendon homeostasis. Second, by depleting *Scx*^{Lin} cells, we mimic the same cellular decline of two "structural ECM-synthesizers" subpopulations of *Scx*^{Lin} cells happening during natural tendon aging, and thus resulting in similar declines of tendon tissue (structure-function and composition) between young DTR and old WT tendons. Based on these findings, we have established a novel model of accelerated ECM aging via depletion of Scx^{Lin} cells. This study is the first to discover that with natural tendon aging, there is a decline in the amount of high turnover rate GPs and PGs, crucial for

maintenance of tendon homeostasis. We also showed that these GPs and PGs are decreased due to the age-related death of tenocytes subclusters that normally produce the above GPs and PGs. Through scRNAseq, we have demonstrated that resident-tissue tendon fibroblasts (tenocytes) have three major and distinct cellular programs, *structural ECM synthesis*, *ECM remodeling and organization*, and *pro-inflammatory and immune responsiveness*. We showed that although both young DTR and aged WT tendons lose the "structural ECM synthesizers" tenocytes, the tenocytes subclusters that are retained between them are programmatically different. Aged WT tendons are composed primarily of "pro-inflammatory" and few "remodelers" tenocytes, which can explain the increased susceptibility of aged tendons to both tendon pathologies and tendon injuries. Finally, we identified a novel cellular subpopulation annotated ("ECM organizer and remodeler", tenocytes 5) with specialized functions in tissue organization and remodeling, which potentially plays significant remodeling roles after injury. These findings motivate and guide future studies focused on therapeutically modulating the tendon cell environment to maintain tendon health during aging and to promote regenerative tendon healing through the lifespan.

Funding: This work was supported in part by NIH/ NIAMS R01AR073169 and R01AR077527 (to AEL). The Histology, Biochemistry and Molecular Imaging (HBMI) Core was supported by NIH/ NIAMS P30AR069655. The content is solely the responsibility of the authors and does not necessarily represent the official views of the National Institutes of Health.

Author contributions: Study conception and design: AK, AEL; Acquisition of data: AK, AECN; Analysis and interpretation of data: AK, AECN, MRB, AEL; Drafting of manuscript: AK, AEL; Revision and approval of manuscript: AK, AECN, MRB, AEL. **Competing interests:** The authors declare that they have no competing interests. **Data and material availability:** All data needed to evaluate the conclusions in the paper are present in the paper or the Supplementary Materials.

References

1. K. T. Best, A. Korcari, K. E. Mora, A. E. Nichols, S. N. Muscat, E. Knapp, M. R. Buckley, A. E. Loiselle, Scleraxis-lineage cell depletion improves tendon healing and disrupts adult tendon homeostasis. *eLife* **10**, (2021).
2. A. J. De Micheli, J. B. Swanson, N. P. Disser, L. M. Martinez, N. R. Walker, D. J. Oliver, B. D. Cosgrove, C. L. Mendias, Single-cell transcriptomic analysis identifies extensive heterogeneity in the cellular composition of mouse Achilles tendons. *Am J Physiol Cell Physiol* **319**, C885-C894 (2020).
3. K. T. Best, A. E. Loiselle, Scleraxis lineage cells contribute to organized bridging tissue during tendon healing and identify a subpopulation of resident tendon cells. *FASEB J* **33**, 8578-8587 (2019).
4. A. R. Kendal, T. Layton, H. Al-Mossawi, L. Appleton, S. Dakin, R. Brown, C. Loizou, M. Rogers, R. Sharp, A. Carr, Multi-omic single cell analysis resolves novel stromal cell populations in healthy and diseased human tendon. *Sci Rep* **10**, 13939 (2020).
5. R. Schweitzer, J. H. Chyung, L. C. Murtaugh, A. E. Brent, V. Rosen, E. N. Olson, A. Lassar, C. J. Tabin, Analysis of the tendon cell fate using Scleraxis, a specific marker for tendons and ligaments. *Development (Cambridge, England)* **128**, 3855-3866 (2001).
6. N. D. Murchison, B. A. Price, D. A. Conner, D. R. Keene, E. N. Olson, C. J. Tabin, R. Schweitzer, Regulation of tendon differentiation by scleraxis distinguishes force-transmitting tendons from muscle-anchoring tendons. *Development* **134**, 2697-2708 (2007).
7. B. A. Pryce, S. S. Watson, N. D. Murchison, J. A. Staverosky, N. Dünker, R. Schweitzer, Recruitment and maintenance of tendon progenitors by TGFbeta signaling are essential for tendon formation. *Development* **136**, 1351-1361 (2009).
8. T. Samiric, M. Z. Ilic, C. J. Handley, Characterisation of proteoglycans and their catabolic products in tendon and explant cultures of tendon. *Matrix Biol* **23**, 127-140 (2004).
9. T. Samiric, M. Z. Ilic, C. J. Handley, Large aggregating and small leucine-rich proteoglycans are degraded by different pathways and at different rates in tendon. *Eur J Biochem* **271**, 3612-3620 (2004).
10. H. Choi, D. Simpson, D. Wang, M. Prescott, A. A. Pitsillides, J. Dudhia, P. D. Clegg, P. Ping, C. T. Thorpe, Heterogeneity of proteome dynamics between connective tissue phases of adult tendon. *Elife* **9**, (2020).
11. K. M. Heinemeier, P. Schjerling, J. Heinemeier, M. B. Moller, M. R. Krogsgaard, T. Grum-Schwensen, M. M. Petersen, M. Kjaer, Radiocarbon dating reveals minimal collagen turnover in both healthy and osteoarthritic human cartilage. *Sci Transl Med* **8**, 346ra390 (2016).
12. S. G. Rees, C. M. Dent, B. Caterson, Metabolism of proteoglycans in tendon. *Scand J Med Sci Sports* **19**, 470-478 (2009).
13. A. Korcari, A. E. Nichols, M. O'Neil, A. E. Loiselle, Ligament and tendon tissue engineering. *Musculoskeletal Tissue Engineering*, 81 (2021).
14. M. Neidlin, A. Korcari, G. Macheras, L. G. Alexopoulos, Cue-signal-response analysis in 3d chondrocyte scaffolds with anabolic stimuli. *Annals of biomedical engineering* **46**, 345-353 (2018).
15. N. L. Millar, K. G. Silbernagel, K. Thorborg, P. D. Kirwan, L. M. Galatz, G. D. Abrams, G. A. C. Murrell, I. B. McInnes, S. A. Rodeo, Tendinopathy. *Nat Rev Dis Primers* **7**, 1 (2021).
16. A. M. Pardes, Z. M. Beach, H. Raja, A. B. Rodriguez, B. R. Freedman, L. J. Soslowsky, Aging leads to inferior Achilles tendon mechanics and altered ankle function in rodents. *J Biomech* **60**, 30-38 (2017).
17. B. K. Connizzo, J. J. Sarver, D. E. Birk, L. J. Soslowsky, R. V. Iozzo, Effect of age and proteoglycan deficiency on collagen fiber re-alignment and mechanical properties in mouse supraspinatus tendon. *J Biomech Eng* **135**, 021019 (2013).
18. M. J. Peffers, C. T. Thorpe, J. A. Collins, R. Eong, T. K. Wei, H. R. Screen, P. D. Clegg, Proteomic analysis reveals age-related changes in tendon matrix composition, with age- and injury-specific matrix fragmentation. *J Biol Chem* **289**, 25867-25878 (2014).
19. R. Gehwolf, A. Wagner, C. Lehner, A. D. Bradshaw, C. Scharler, J. A. Niestrawska, G. A. Holzapfel, H. C. Bauer, H. Tempfer, A. Traweger, Pleiotropic roles of the matricellular protein Sparc in tendon maturation and ageing. *Sci Rep* **6**, 32635 (2016).
20. T. Wang, A. Wagner, R. Gehwolf, W. Yan, F. S. Passini, C. Thien, N. Weissenbacher, Z. Lin, C. Lehner, H. Teng, C. Wittner, Q. Zheng, J. Dai, M. Ni, A. Wang, J. Papadimitriou, T. Leys, R. S. Tuan, S. Senck, J. G. Snedeker, H. Tempfer, Q. Jiang, M. H. Zheng, A. Traweger, Load-induced regulation of tendon homeostasis by SPARC, a genetic predisposition factor for tendon and ligament injuries. *Sci Transl Med* **13**, (2021).
21. T. Y. Kostrominova, S. V. Brooks, Age-related changes in structure and extracellular matrix protein expression levels in rat tendons. *Age (Dordr)* **35**, 2203-2214 (2013).

22. R. C. Marqueti, J. L. Q. Durigan, A. J. S. Oliveira, M. S. Mekaro, V. Guzzoni, A. A. Aro, E. R. Pimentel, H. S. Selistre-de-Araujo, Effects of aging and resistance training in rat tendon remodeling. *FASEB J* **32**, 353-368 (2018).
23. A. Korcari, A. E. Loiselle, M. R. Buckley, Characterization of scar tissue biomechanics during adult murine flexor tendon healing. *bioRxiv*, 2021.2011.2009.467960 (2021).
24. H. Riel, C. F. Lindstrom, M. S. Rathleff, M. B. Jensen, J. L. Olesen, Prevalence and incidence rate of lower-extremity tendinopathies in a Danish general practice: a registry-based study. *BMC Musculoskelet Disord* **20**, 239 (2019).
25. A. A. Dunkman, M. R. Buckley, M. J. Mienaltowski, S. M. Adams, S. J. Thomas, L. Satchell, A. Kumar, L. Pathmanathan, D. P. Beason, R. V. Iozzo, D. E. Birk, L. J. Soslowsky, Decorin expression is important for age-related changes in tendon structure and mechanical properties. *Matrix biology : journal of the International Society for Matrix Biology* **32**, 3-13 (2013).
26. E. Ippolito, P. G. Natali, F. Postacchini, L. Accinni, C. De Martino, Morphological, immunochemical, and biochemical study of rabbit achilles tendon at various ages. *JBJS* **62**, 583-598 (1980).
27. B. K. Connizzo, L. Han, D. E. Birk, L. J. Soslowsky, Collagen V-heterozygous and -null supraspinatus tendons exhibit altered dynamic mechanical behaviour at multiple hierarchical scales. *Interface Focus* **6**, 20150043 (2016).
28. T. Sakabe, K. Sakai, T. Maeda, A. Sunaga, N. Furuta, R. Schweitzer, T. Sasaki, T. Sakai, Transcription factor scleraxis vitally contributes to progenitor lineage direction in wound healing of adult tendon in mice. *J Biol Chem* **293**, 5766-5780 (2018).
29. J. E. Ackerman, I. Bah, J. H. Jonason, M. R. Buckley, A. E. Loiselle, Aging does not alter tendon mechanical properties during homeostasis, but does impair flexor tendon healing. *J Orthop Res* **35**, 2716-2724 (2017).
30. K. T. Best, A. Korcari, K. E. Mora, A. E. Nichols, S. N. Muscat, E. Knapp, M. R. Buckley, A. E. Loiselle, Scleraxis-lineage cell depletion improves tendon healing and disrupts adult tendon homeostasis. *Elife* **10**, e62203 (2021).
31. C. A. Schneider, W. S. Rasband, K. W. Eliceiri, NIH Image to ImageJ: 25 years of image analysis. *Nature Methods* **9**, 671-675 (2012).
32. D. P. Lobo, A. M. Wemyss, D. J. Smith, A. Straube, K. B. Betteridge, A. H. J. Salmon, R. R. Foster, H. E. Elhegni, S. C. Satchell, H. A. Little, R. Pacheco-Gómez, M. J. Simmons, M. R. Hicks, D. O. Bates, A. Rodger, T. R. Dafforn, K. P. Arkill, Direct detection and measurement of wall shear stress using a filamentous bio-nanoparticle. *Nano Research* **8**, 3307-3315 (2015).
33. H. Mi, D. Ebert, A. Muruganujan, C. Mills, L.-P. Albou, T. Mushayamaha, P. D. Thomas, PANTHER version 16: a revised family classification, tree-based classification tool, enhancer regions and extensive API. *Nucleic Acids Research* **49**, D394-D403 (2020).
34. W. Huang da, B. T. Sherman, R. A. Lempicki, Systematic and integrative analysis of large gene lists using DAVID bioinformatics resources. *Nat Protoc* **4**, 44-57 (2009).
35. D. Szklarczyk, A. L. Gable, D. Lyon, A. Junge, S. Wyder, J. Huerta-Cepas, M. Simonovic, N. T. Doncheva, J. H. Morris, P. Bork, L. J. Jensen, C. V. Mering, STRING v11: protein-protein association networks with increased coverage, supporting functional discovery in genome-wide experimental datasets. *Nucleic Acids Res* **47**, D607-D613 (2019).
36. R. O. Hynes, A. Naba, Overview of the matrisome--an inventory of extracellular matrix constituents and functions. *Cold Spring Harb Perspect Biol* **4**, a004903 (2012).
37. T. Stuart, A. Butler, P. Hoffman, C. Hafemeister, E. Papalexi, W. M. Mauck, 3rd, Y. Hao, M. Stoeckius, P. Smibert, R. Satija, Comprehensive Integration of Single-Cell Data. *Cell* **177**, 1888-1902 e1821 (2019).
38. X. Zhang, Y. Lan, J. Xu, F. Quan, E. Zhao, C. Deng, T. Luo, L. Xu, G. Liao, M. Yan, Y. Ping, F. Li, A. Shi, J. Bai, T. Zhao, X. Li, Y. Xiao, CellMarker: a manually curated resource of cell markers in human and mouse. *Nucleic Acids Res* **47**, D721-D728 (2019).
39. J. E. Ackerman, A. E. Loiselle, Murine Flexor Tendon Injury and Repair Surgery. *J Vis Exp*, (2016).
40. V. Tam, P. Chen, A. Yee, N. Solis, T. Klein, M. Kudelko, R. Sharma, W. C. Chan, C. M. Overall, L. Haglund, P. C. Sham, K. S. E. Cheah, D. Chan, DIPPER, a spatiotemporal proteomics atlas of human intervertebral discs for exploring ageing and degeneration dynamics. *Elife* **9**, (2020).
41. A. Butler, P. Hoffman, P. Smibert, E. Papalexi, R. Satija, Integrating single-cell transcriptomic data across different conditions, technologies, and species. *Nat Biotechnol* **36**, 411-420 (2018).
42. Y. Sugiyama, K. Naito, K. Goto, Y. Kojima, A. Furuhata, M. Igarashi, I. Nagaoka, K. Kaneko, Effect of aging on the tendon structure and tendon-associated gene expression in mouse foot flexor tendon. *Biomed Rep* **10**, 238-244 (2019).

43. R. L. Stanley, R. A. Fleck, D. L. Becker, A. E. Goodship, J. R. Ralphs, J. C. Patterson-Kane, Gap junction protein expression and cellularity: comparison of immature and adult equine digital tendons. *J Anat* **211**, 325-334 (2007).
44. Z. Yan, H. Yin, C. Brochhausen, C. G. Pfeifer, V. Alt, D. Docheva, Aged Tendon Stem/Progenitor Cells Are Less Competent to Form 3D Tendon Organoids Due to Cell Autonomous and Matrix Production Deficits. *Front Bioeng Biotechnol* **8**, 406 (2020).
45. E. Ippolito, P. G. Natali, F. Postacchini, L. Accinni, C. De Martino, Morphological, immunochemical, and biochemical study of rabbit achilles tendon at various ages. *J Bone Joint Surg Am* **62**, 583-598 (1980).
46. H. Watanabe, K. Kimata, S. Line, D. Strong, L. Y. Gao, C. A. Kozak, Y. Yamada, Mouse cartilage matrix deficiency (cmd) caused by a 7 bp deletion in the aggrecan gene. *Nat Genet* **7**, 154-157 (1994).
47. H. Watanabe, K. Nakata, K. Kimata, I. Nakanishi, Y. Yamada, Dwarfism and age-associated spinal degeneration of heterozygote cmd mice defective in aggrecan. *Proc Natl Acad Sci U S A* **94**, 6943-6947 (1997).
48. M. A. Batista, H. T. Nia, P. Onnerfjord, K. A. Cox, C. Ortiz, A. J. Grodzinsky, D. Heinegard, L. Han, Nanomechanical phenotype of chondroadherin-null murine articular cartilage. *Matrix Biol* **38**, 84-90 (2014).
49. L. Hessle, G. A. Stordalen, C. Wenglen, C. Petzold, E. Tanner, S. H. Brorson, E. S. Baekkevold, P. Onnerfjord, F. P. Reinholt, D. Heinegard, The skeletal phenotype of chondroadherin deficient mice. *PLoS One* **8**, e63080 (2014).
50. E. Poschl, U. Schlotzer-Schrehardt, B. Brachvogel, K. Saito, Y. Ninomiya, U. Mayer, Collagen IV is essential for basement membrane stability but dispensable for initiation of its assembly during early development. *Development* **131**, 1619-1628 (2004).
51. D. Cosgrove, D. T. Meehan, J. A. Grunkemeyer, J. M. Kornak, R. Sayers, W. J. Hunter, G. C. Samuelson, Collagen COL4A3 knockout: a mouse model for autosomal Alport syndrome. *Genes Dev* **10**, 2981-2992 (1996).
52. J. T. Hecht, L. D. Nelson, E. Crowder, Y. Wang, F. F. Elder, W. R. Harrison, C. A. Francomano, C. K. Prange, G. G. Lennon, M. Deere, et al., Mutations in exon 17B of cartilage oligomeric matrix protein (COMP) cause pseudoachondroplasia. *Nat Genet* **10**, 325-329 (1995).
53. H. Geng, S. Carlsen, K. S. Nandakumar, R. Holmdahl, A. Aspberg, A. Oldberg, R. Mattsson, Cartilage oligomeric matrix protein deficiency promotes early onset and the chronic development of collagen-induced arthritis. *Arthritis Res Ther* **10**, R134 (2008).
54. K. Tiedemann, I. Boraschi-Diaz, I. Rajakumar, J. Kaur, P. Roughley, D. P. Reinhardt, S. V. Komarova, Fibrillin-1 directly regulates osteoclast formation and function by a dual mechanism. *J Cell Sci* **126**, 4187-4194 (2013).
55. L. Y. Sakai, D. R. Keene, M. Renard, J. De Backer, FBN1: The disease-causing gene for Marfan syndrome and other genetic disorders. *Gene* **591**, 279-291 (2016).
56. S. Dex, P. Alberton, L. Willkomm, T. Sollradl, S. Bago, S. Milz, M. Shakibaei, A. Ignatius, W. Bloch, H. Clausen-Schaumann, C. Shukunami, M. Schieker, D. Docheva, Tenomodulin is Required for Tendon Endurance Running and Collagen I Fibril Adaptation to Mechanical Load. *EBioMedicine* **20**, 240-254 (2017).
57. M. Barbier, M. S. Gross, M. Aubart, N. Hanna, K. Kessler, D. C. Guo, L. Tosolini, B. Ho-Tin-Noe, E. Regalado, M. Varret, M. Abifadel, O. Milleron, S. Odent, S. Dupuis-Girod, L. Faivre, T. Edouard, Y. Dulac, T. Busa, L. Gouya, D. M. Milewicz, G. Jondeau, C. Boileau, MFAP5 loss-of-function mutations underscore the involvement of matrix alteration in the pathogenesis of familial thoracic aortic aneurysms and dissections. *Am J Hum Genet* **95**, 736-743 (2014).
58. R. Kokenyesi, L. C. Armstrong, A. Agah, R. Artal, P. Bornstein, Thrombospondin 2 deficiency in pregnant mice results in premature softening of the uterine cervix. *Biol Reprod* **70**, 385-390 (2004).
59. A. N. Qabar, Z. Lin, F. W. Wolf, K. S. O'Shea, J. Lawler, V. M. Dixit, Thrombospondin 3 is a developmentally regulated heparin binding protein. *Journal of Biological Chemistry* **269**, 1262-1269 (1994).
60. D. H. Lee, J. H. Oh, J. H. Chung, Glycosaminoglycan and proteoglycan in skin aging. *J Dermatol Sci* **83**, 174-181 (2016).
61. Y. Ariosa-Morejon, A. Santos, R. Fischer, S. Davis, P. Charles, R. Thakker, A. K. Wann, T. L. Vincent, Age-dependent changes in protein incorporation into collagen-rich tissues of mice by in vivo pulsed SILAC labelling. *Elife* **10**, (2021).
62. M. C. McCabe, R. C. Hill, K. Calderone, Y. Cui, Y. Yan, T. Quan, G. J. Fisher, K. C. Hansen, Alterations in extracellular matrix composition during aging and photoaging of the skin. *Matrix Biol Plus* **8**, 100041 (2020).
63. G. P. Riley, R. L. Harrall, C. R. Constant, M. D. Chard, T. E. Cawston, B. L. Hazleman, Glycosaminoglycans of human rotator cuff tendons: changes with age and in chronic rotator cuff tendinitis. *Ann Rheum Dis* **53**, 367-376 (1994).
64. J. E. Ackerman, K. T. Best, S. N. Muscat, C.-L. Wu, A. E. Loiselle, (2021).
65. M. Akbar, L. MacDonald, L. A. N. Crowe, K. Carlberg, M. Kurowska-Stolarska, P. L. Stahl, S. J. B. Snelling, I. B. McInnes, N. L. Millar, Single cell and spatial transcriptomics in human tendon disease indicate dysregulated immune homeostasis. *Ann Rheum Dis* **80**, 1494-1497 (2021).

66. C. Lehner, G. Spitzer, R. Gehwolf, A. Wagner, N. Weissenbacher, C. Deininger, K. Emmanuel, F. Wichlas, H. Tempfer, A. Traweger, Tenophages: a novel macrophage-like tendon cell population expressing CX3CL1 and CX3CR1. *Dis Model Mech* **12**, (2019).
67. L. Sole-Boldo, G. Raddatz, S. Schutz, J. P. Mallm, K. Rippe, A. S. Lonsdorf, M. Rodriguez-Paredes, F. Lyko, Single-cell transcriptomes of the human skin reveal age-related loss of fibroblast priming. *Commun Biol* **3**, 188 (2020).
68. C. Franceschi, M. Bonafe, S. Valensin, F. Olivieri, M. De Luca, E. Ottaviani, G. De Benedictis, Inflamm-aging. An evolutionary perspective on immunosenescence. *Ann N Y Acad Sci* **908**, 244-254 (2000).
69. S. Ma, S. Sun, J. Li, Y. Fan, J. Qu, L. Sun, S. Wang, Y. Zhang, S. Yang, Z. Liu, Z. Wu, S. Zhang, Q. Wang, A. Zheng, S. Duo, Y. Yu, J. C. I. Belmonte, P. Chan, Q. Zhou, M. Song, W. Zhang, G. H. Liu, Single-cell transcriptomic atlas of primate cardiopulmonary aging. *Cell Res* **31**, 415-432 (2021).
70. S. Ma, S. Sun, L. Geng, M. Song, W. Wang, Y. Ye, Q. Ji, Z. Zou, S. Wang, X. He, W. Li, C. R. Esteban, X. Long, G. Guo, P. Chan, Q. Zhou, J. C. I. Belmonte, W. Zhang, J. Qu, G. H. Liu, Caloric Restriction Reprograms the Single-Cell Transcriptional Landscape of Rattus Norvegicus Aging. *Cell* **180**, 984-1001 e1022 (2020).
71. M. C. Salzer, A. Lafzi, A. Berenguer-Llergo, C. Youssif, A. Castellanos, G. Solanas, F. O. Peixoto, C. Stephan-Otto Attolini, N. Prats, M. Aguilera, J. Martin-Caballero, H. Heyn, S. A. Benitah, Identity Noise and Adipogenic Traits Characterize Dermal Fibroblast Aging. *Cell* **175**, 1575-1590 e1522 (2018).
72. S. Agarwal, S. J. Loder, D. Cholok, J. Peterson, J. Li, C. Breuler, R. Cameron Brownley, H. Hsin Sung, M. T. Chung, N. Kamiya, S. Li, B. Zhao, V. Kaartinen, T. A. Davis, A. T. Qureshi, E. Schipani, Y. Mishina, B. Levi, Scleraxis-Lineage Cells Contribute to Ectopic Bone Formation in Muscle and Tendon. *Stem Cells* **35**, 705-710 (2017).
73. Y. Yoshimoto, A. Takimoto, H. Watanabe, Y. Hiraki, G. Kondoh, C. Shukunami, Scleraxis is required for maturation of tissue domains for proper integration of the musculoskeletal system. *Sci Rep* **7**, 45010 (2017).

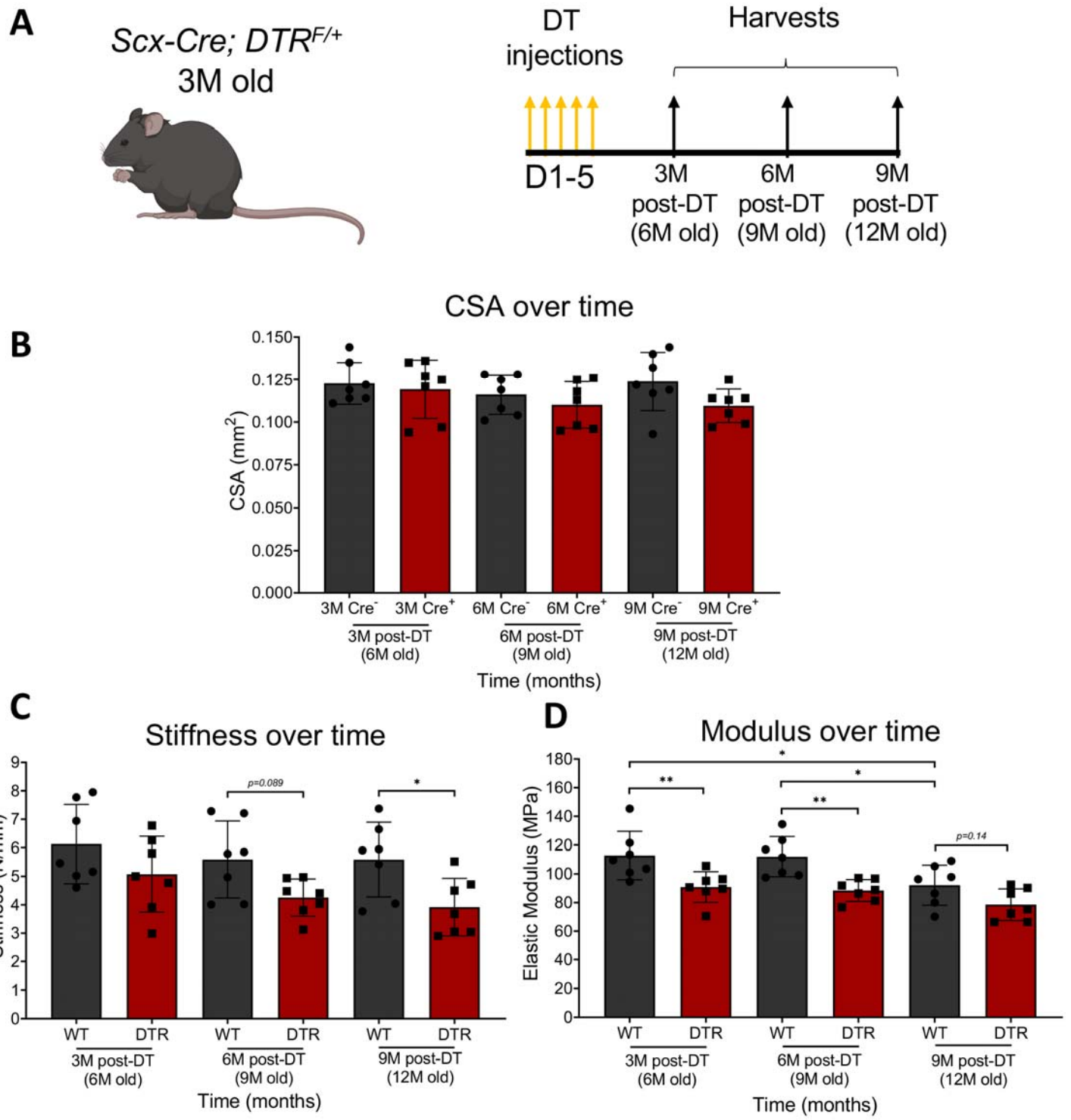

Supplemental figure 1. Depletion of *Scx*^{Lin} cells significantly impairs tendon structural and material properties. Timeline of DT injections and tissue harvesting **(A)**. Quantification of CSA **(B)**, stiffness **(C)**, and elastic modulus **(D)** of WT and DTR tendons at 3, 6, and 9 months post-depletion. CSA, stiffness, and elastic modulus between genotype (WT or DTR) and timepoint (3M, 6M, or 9M). N=3-5 per genotype. Two-way ANOVA with Sidak's multiple comparisons test used to assess statistical significance of CSA, stiffness, and elastic modulus, * indicates $p<0.05$; ** indicates $p<0.01$; *** indicates $p<0.001$; **** indicates $p<0.0001$.

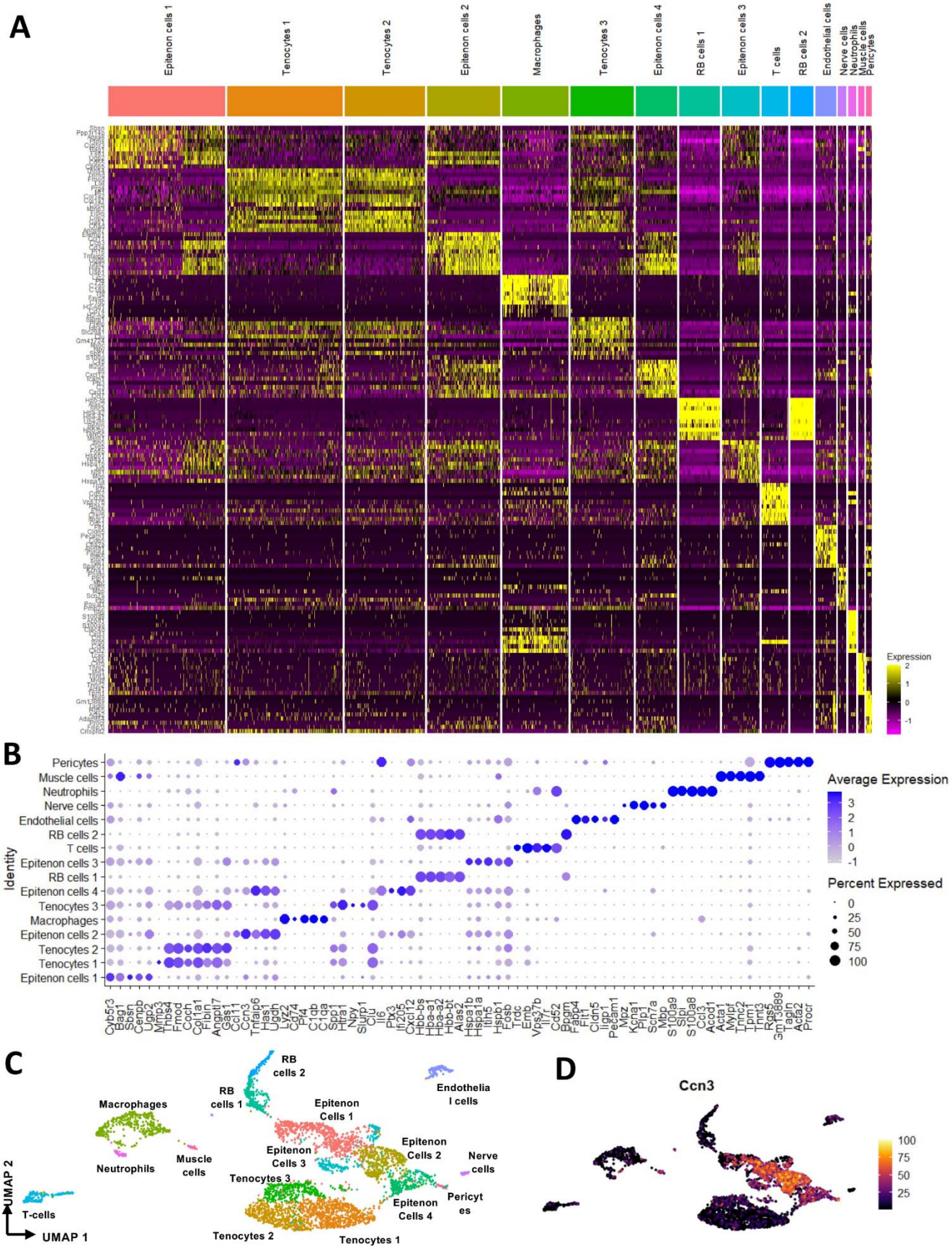

Supplemental figure 2. Annotation of scRNAseq-based identified cell clusters in the integrated data. Heatmap of top 15 DEGs for each cluster **(A)**. Dot plot with the top 5 DEGs per cluster **(B)**. **(C)** UMAP with all different clusters annotated based on **(A, B). (D)** Feature plot of the epitenon marker *Ccn3* being expressed by the epitenon sub-clusters.

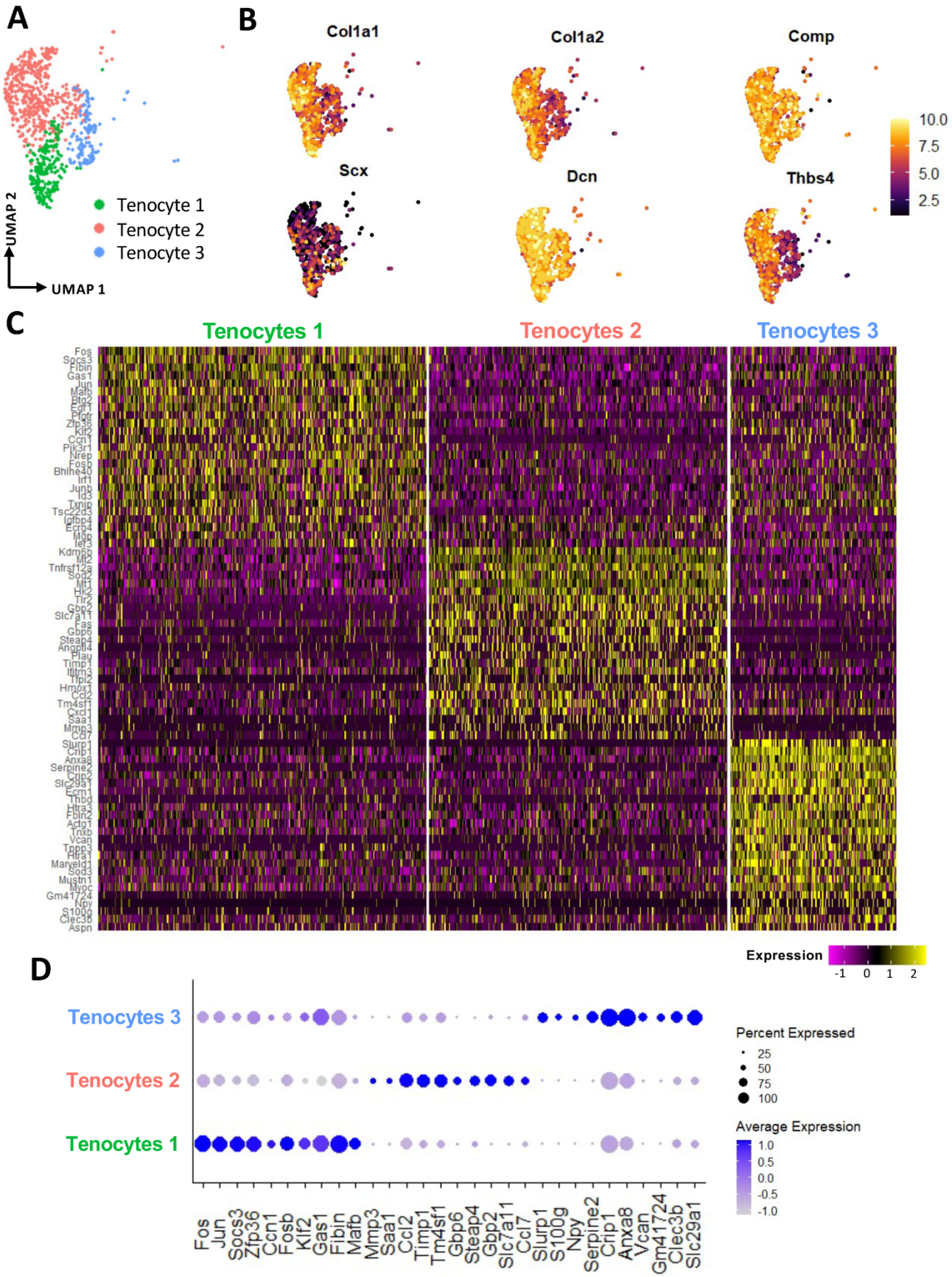

Supplemental figure 3. Annotation of scRNAseq-based identified cell clusters in only young WT tendons. (A) UMAP of the three tenocyte subpopulations from the young WT group. **(B)** Feature Plot of different tendon-related markers in the three tenocyte subpopulations. **(C)** Heatmap of top 25 DEGs for each cluster. **(D)** Dot plot with the top 10 DEGs per cluster.

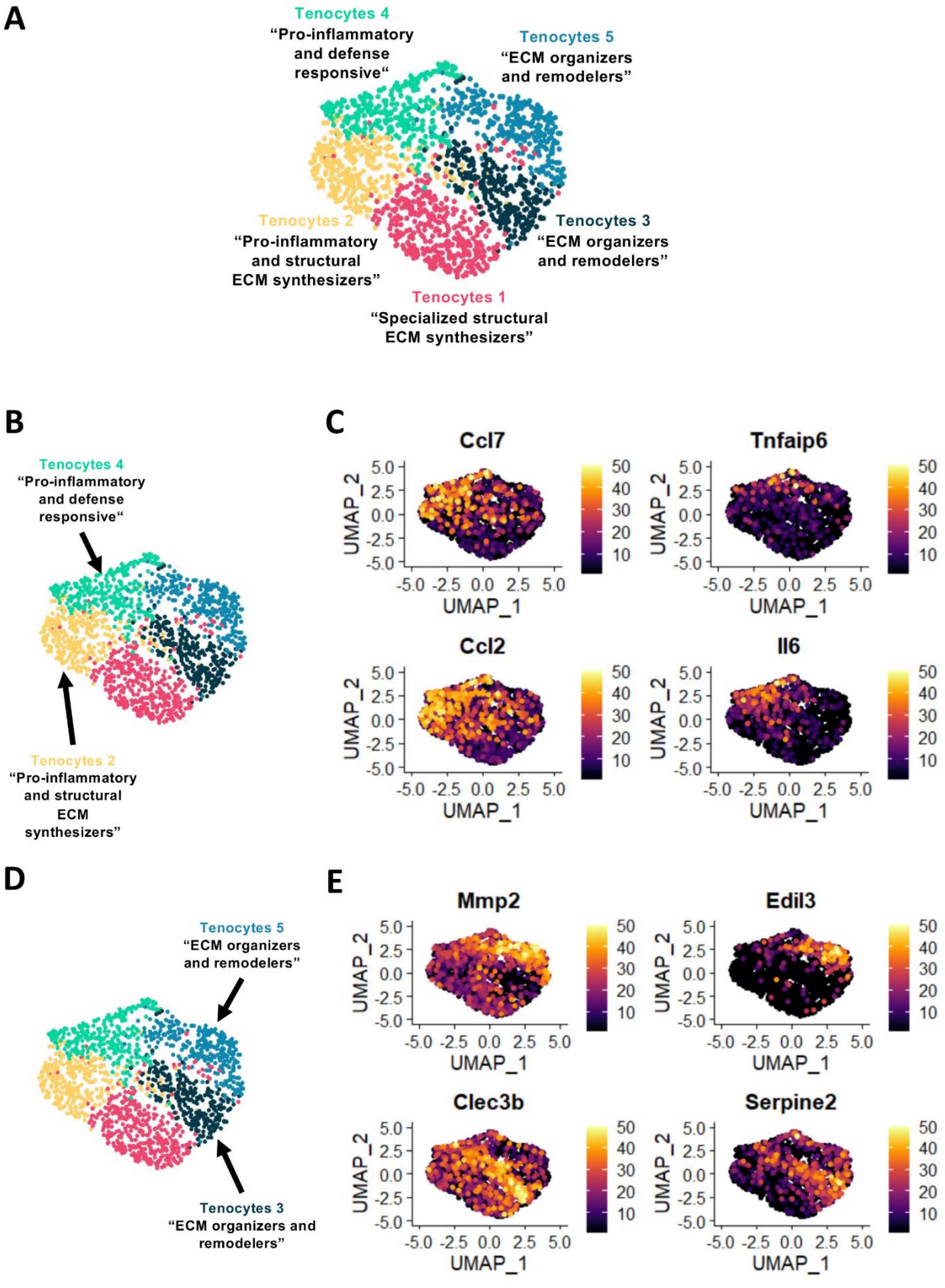

Supplemental figure 4. Visualization of inflammatory-based and remodeling-based markers in tenocytes 2, 4 and 3, 5, respectively. Annotated tenocytes subpopulations **(A)**. UMAP visualization of inflammatory-based tenocytes 2 and 4 **(B).** Inflammatory-based markers (*Ccl7, Tnfaip6, Ccl2, Il6)* highly expressed in tenocytes 2, 4 **(C).** UMAP visualization of tissue organization and remodeling tenocytes 3 and 5 **(D).** Tissue organization and remodeling specific markers (*Mmp2, Edil3, Clec3b, Serpine2*) highly expressed in tenocytes 3 and 5 **(E)**.

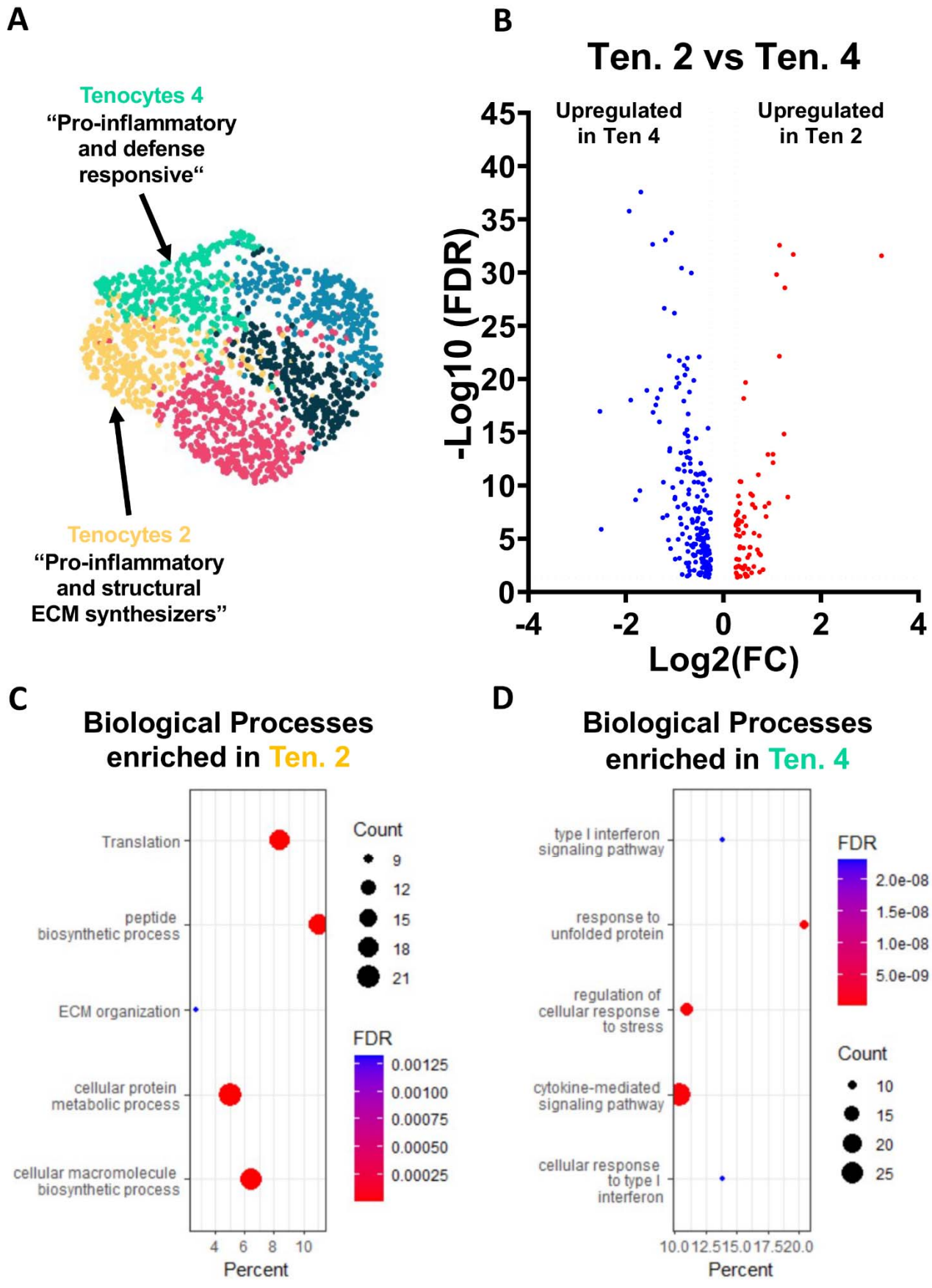

Supplemental figure 5. Tenocytes 2 are more biosynthetic and less inflammatory than tenocytes 4. (A) UMAP visualization of inflammatory-based tenocytes 2 and 4. **(B)** Volcano plot of the DEGs between ten.2 and ten. 4. **(C)** BPs enriched in ten.2 based on DEGs upregulated in ten. 2 relative to ten. 4. **(D)** BPs enriched in ten. 4 based on DEGs upregulated in ten. 4 relative to ten. 2.

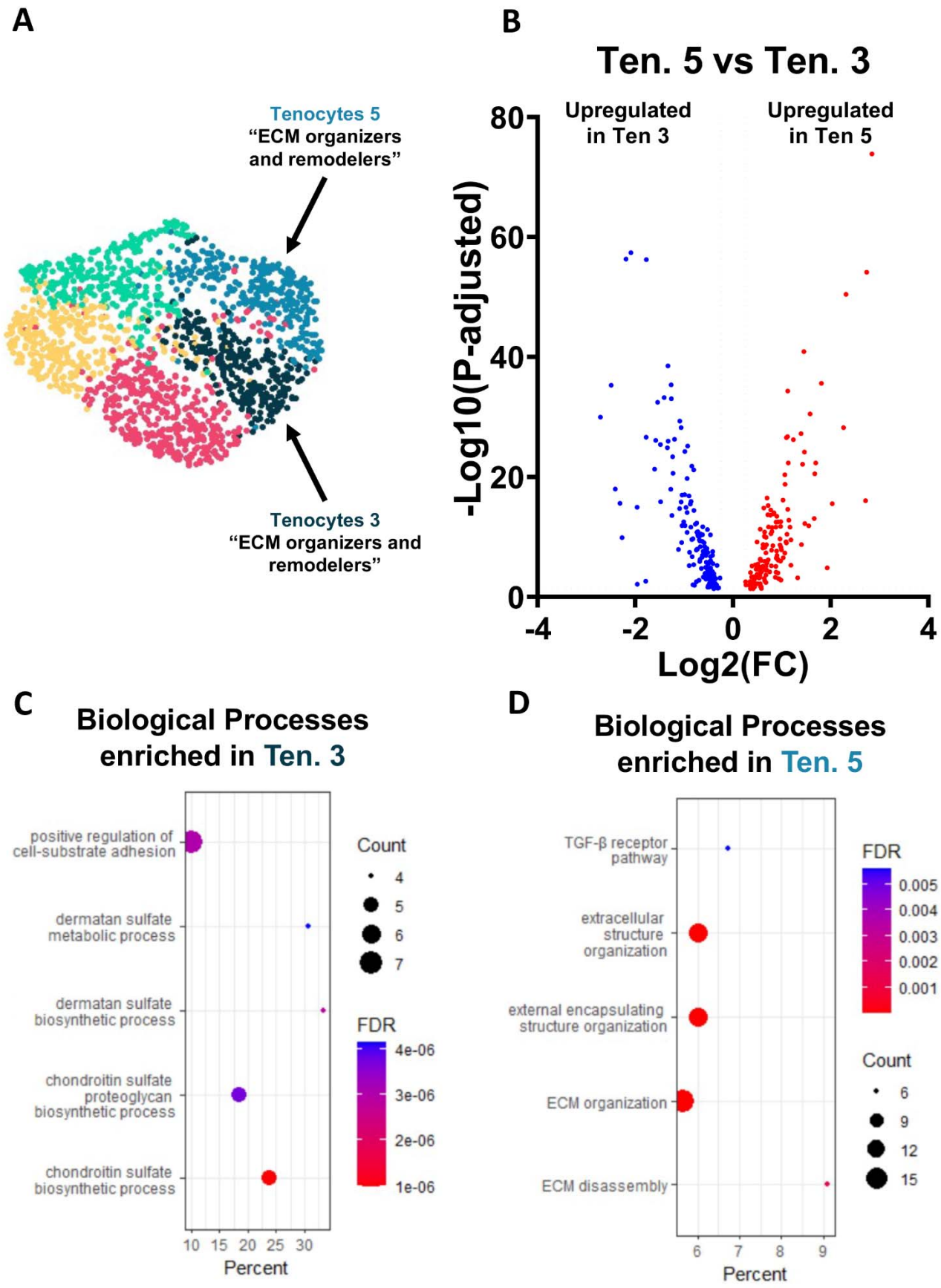

Supplemental figure 6. Tenocytes 5 are organizational specific while tenocytes 3 are biosynthetic specific. (A) UMAP visualization of inflammatory-based tenocytes 5 and 3. **(B)** Volcano plot of the DEGs between ten. 5 and ten. 3. **(C)** BPs enriched in ten.5 based on DEGs upregulated in ten. 5 relative to ten. 3. **(D)** BPs enriched in ten. 3 based on DEGs upregulated in ten. 3 relative to ten. 5.

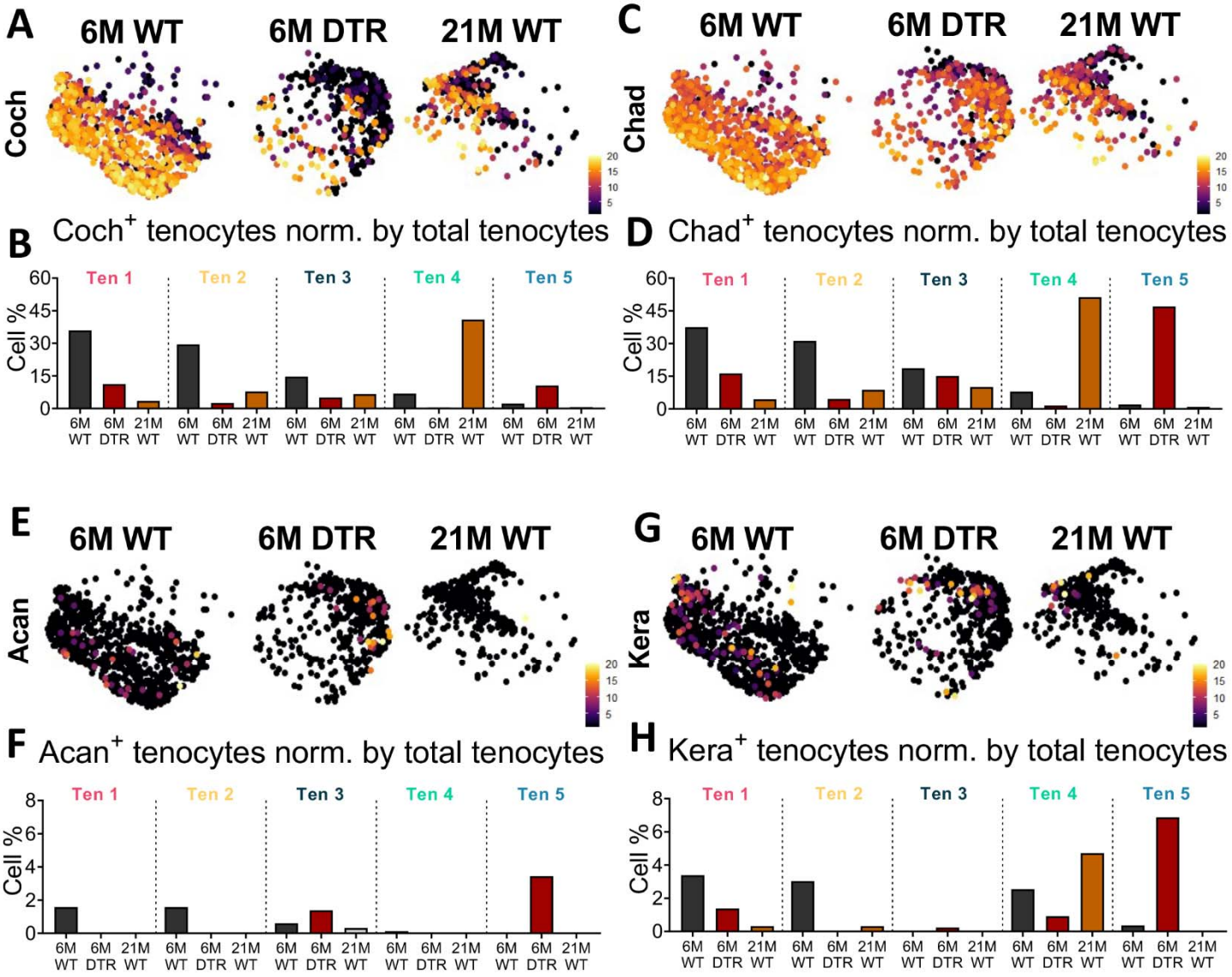

Supplemental figure 7. Potential regulators of ECM homeostasis are decreased in depleted and aged tendons in terms of tenocyte number positive for those and expression levels. (A) UMAP showing cells that are *Coch*$^+$ WT, DTR, and 21M WT groups. **(B)** Quantification of *Coch*$^+$ cell density for each tenocyte subpopulation normalized by the total number of tenocytes for each respective group. **(C)** UMAP showing cells that are *Chad*$^+$ WT, DTR, and 21M WT groups. **(D)** Quantification of *Chad*$^+$ cell density for each tenocyte subpopulation normalized by the total number of tenocytes for each respective group. **(E)** UMAP showing cells that are *Acan*$^+$ in WT, DTR, and 21M WT groups. **(F)** Quantification of *Acan*$^+$ cell density for each tenocyte subpopulation normalized by the total number of tenocytes for each respective group. **(G)** UMAP showing cells that are *Kera*$^+$ in WT, DTR, and 21M WT groups. **(H)** Quantification of *Kera*$^+$ cell density for each tenocyte subpopulation normalized by the total number of tenocytes for each respective group.